DETECTING LONG-TERM TRENDS IN WATER QUALITY PARAMETERS USING REMOTE SENSING TECHNIQUES

BY

JINNA HYEON LARKIN

THESIS

Submitted in partial fulfillment of the requirements
for the degree of Master of Science in Natural Resources and Environmental Sciences
in the Graduate College of the
University of Illinois at Urbana-Champaign, 2014

Urbana, Illinois

Master's Committee:

Assistant Professor Jennifer Fraterrigo, Chair
Assistant Professor Jonathan Greenberg
Professor Mark David
Professor Bruce Rhoads

Abstract

Estuarine systems have undergone extensive alteration as a result of anthropogenic activities. Detecting the magnitude of alteration and anticipating future change are crucial for managing these systems, but challenging because they require long-term records of chemical and biological water quality, which are not widely available. Moderate resolution remote sensing imagery is a rich and temporally extensive source of information about ecological systems and may be useful for detecting past and predicting future changes in estuarine ecosystems. I evaluated the use of moderate resolution Landsat-5 TM imagery for estimating three indicators of water quality: Secchi depth (SDD), chlorophyll-*a* concentration (Chl-a), and dissolved organic carbon (DOC). Reflectance and *in situ* data were collected within seven days of satellite overpass and used to build calibration models for SDD, Chl-a, and DOC in the Hudson River Estuary, New York. The accuracy of model estimates was evaluated using a validation dataset and water quality indicators were mapped for the period 2005-2008. The correlation between predicted and observed values was highest for SDD and Chl-a (r=0.62 and 0.41, resp.) and lowest for DOC (r=0.26). The root mean squared error between predicted and observed values was 20.24 cm for SDD, 0.49 ug/L for Chl-a) and 0.24 mg/L for DOC. While predictive maps indicate that turbidity decreased and chlorophyll-*a* concentration increased with distance downstream in 2005, there were no apparent spatial gradients for these parameters by 2008. Further analysis suggests that discrepancies between predicted and observed values were likely due to asynchronous collection of satellite and *in situ* data that reduce the sensitivity of models to the dynamic nature of estuarine systems. Overall, these findings suggest a strong potential for Landsat TM imagery to be used to estimate SDD and Chl-a for this area, whereas higher resolution sensor and synchronous satellite and *in situ* data may be needed to improve the accuracy of satellite-based DOC estimates for the Hudson River.

ACKNOWLEDGMENTS

This project would not have been possible without the support of many people. Many thanks to my adviser, Jennifer Fraterrigo, who read my numerous revisions and helped make some sense of the confusion. Also thanks to my committee members, Jonathan Greenberg, Mark David, and Bruce Rhoads, who offered guidance and support. Thanks to the Department of Natural Resources for awarding me the Graduate Award for Excellence in Research, providing me with the financial means to complete this project, as well as Karen Claus for her fast turn-around with final revisions.

And finally, thanks to my parents, labmates, fellow grad students, and numerous friends who endured this long process with me, always offering support and love.

TABLE OF CONTENTS

Chapter 1: Introduction

Estuarine systems provide important resources and services to wildlife and humans alike. They have long since served as ideal areas for human settlements as well as a vital habitat for a variety of fish and water fowl (Lotze et al. 2006, Barbier et al. 2010). Many estuaries also have great economic value as an invaluable resource for the fishing industry (Lotze et al. 2006, Barbier et al. 2010). As heavily used aquatic environments, estuarine systems have undergone extensive alteration that has greatly accelerated over the past century (Lotze et al. 2006). The Hudson River ecosystem, for example, has long served as an important passage for the transport of people and goods and has been appreciably altered by anthropogenic activities. Years of pollution by local industry has led to a significant deterioration in water quality and high concentrations of toxins in fish populations, resulting in fishery decline and the need for remediation. The introduction of the invasive *Dreissena polymorpha*, more commonly known as the zebra mussel, caused the near disappearance of native mussels due to an increased consumption of phytoplankton and zooplankton (Strayer and Smith 2001). Such degradation has also lowered the resilience of the Hudson to other stressors like climate change and atmospheric pollution, with increased nitrogen deposition being linked to terrestrially derived DOC levels nearly doubling between 1989 and 2005 (Findlay 2005, Lotze et al. 2006). Consequently, estuarine systems and the functions they provide are projected to change in the future despite efforts aimed at restoring and protecting them (Lotze et al. 2006).

Evaluating temporal changes in the water quality of estuarine systems can be important for detecting and anticipating shifts in overall ecosystem health. There are a number of measurable variables that can serve as indicators of water quality. Secchi depth is a measure of the concentration of light attenuating particles in water, and long-term records of Secchi depth are useful for detecting changes in the transparency of the water column (Borkman and Smayda 1998, Fleming-Lehtinen and Laamanen 2012). This is significant because transparency impacts the light regimes of water bodies,

which in turn affect phytoplankton communities and primary production in deep estuaries by determining the depth of the photic layer and the habitat extent of primary producers (Borkman and Smayda 1998, Fleming-Lehtinen and Laamanen 2012). Transparency also affects the relative contribution of phytoplankton and submersed aquatic vegetation to primary production, and is thus correlated with eutrophication and phytoplankton biomass, as well as the occurrence of phytoplankton blooms (Borkman and Smayda 1998, Gallegos et al. 2011, Fleming-Lehtinen and Laamanen 2012). Chlorophyll-*a* is found in photosynthetic algae and cyanobacteria an its concentration is a proxy for phytoplankton biomass (Paerl et al. 2003). As such, chlorophyll-*a* concentration is a valuable indicator of primary production rates in aquatic systems, as well as a measure of eutrophication status (Hays et al. 2005, McQuatters-Gollop et al. 2007, Abreu et al. 2010). Dissolved organic carbon (DOC) is an essential constituent of aquatic ecosystems, serving as a major form of organic matter (Findlay and Sinsabaugh 2003) and stabilizing pH through organic acid buffering capacity (Ceppi et al. 1999, García-Gil et al. 2004). It plays an intricate role in the metabolism of aquatic systems, especially the food web by serving as an energy source for many aquatic microorganisms and thus fueling the microbial loop (Findlay et al. 1993, Findlay and Sinsabaugh 2003, Yamashita and Jaffé 2008, Yamashita et al. 2010). DOC can also influence the availability of other dissolved nutrients and metals by aiding in the conversion of inorganic nutrients to organic forms in nutrient-rich waters and providing a substrate for trace metal complexation (Findlay and Sinsabaugh 2003, Yamashita et al. 2010). Finally, terrestrially derived DOC can modify the optical properties of water by absorbing ultra-violet light, which, by affecting transparency, can offer protection to some aquatic organisms and influence where they reside in the water column (Frenette et al. 2003, Lennon 2004, Roulet and Moore 2006, Hayakawa and Sugiyama 2008).

Comprehensive, long-term water quality records are needed to evaluate temporal changes in estuarine systems, but are not widely available. Major advances in technology, however, have led

scientists to begin remotely sensing water quality indicators, allowing for large amounts of data to be collected rapidly and cost effectively. Water color depends on the absorption and scattering of light by organic and inorganic constituents present in the water column (Bukata 2005). For inland and coastal waters, including estuaries, changes in phytoplankton and detritus, terrestrially derived suspended particulate inorganic matter, color dissolved organic matter (CDOM), and benthic substrate can result in changes in the reflected visible radiation of the water, which remote sensing devices, ranging from spectrophotometers to space-based sensors, are capable of detecting (Lavery et al. 1993, Pattiaratchi et al. 1994, Ruddick et al. 2001, Bukata 2005). Several past studies have employed remote sensing imagery to measure and predict SDD, Chl-a, and DOC in aquatic systems (Lillesand et al. 1983, Lathrop and Lillesand 1986, Lathrop 1992, Baban 1993, Gitelson et al. 1993, Lavery et al. 1993, Pattiaratchi et al. 1994, Baban 1997, Giardino et al. 2001, Ruddick et al. 2001, Dekker et al. 2002, Kloiber et al. 2002a, Kloiber et al. 2002b, Brando and Dekker 2003, Hirtle and Rencz 2003, Chipman et al. 2004, Hellweger et al. 2004, Wang et al. 2004, Brezonik et al. 2005, Doxaran et al. 2005, Kutser et al. 2005a, Kutser et al. 2005b, Wang et al. 2006, Giardino et al. 2007, Kabbara et al. 2008, Kallio et al. 2008, Olmanson et al. 2008, Chernetskiy et al. 2009, Hadjimitsis and Clayton 2009, Kutser et al. 2009). Many of these studies use imagery that has high spatial and spectral resolution because sensors with narrow bands are more sensitive to subtle changes in reflectance, which is helpful when working in complex aquatic systems. However, this heightened sensitivity can also lead to a lower signal-to-noise ratio (SNR) because water enhances scattering of radiation from sunlight both on the surface and within the water column, making it difficult to get a clear signal. The temporal resolution of imagery can also be important because water quality conditions can change drastically over a short period of time (Hellweger et al. 2004).

There are many recent examples of the application of remote sensing technology in water quality studies. For instance, data collected by sensors aboard the Satellite Pour l'Observation de la Terre (SPOT) have been used to determine suspended matter concentrations in various lakes, allowing

for multi-temporal, multi-site comparison of total suspended material (Dor and Ben-Yosef 1996, Dekker et al. 2002, Doxaran et al. 2002, Doxaran et al. 2003, Doxaran et al. 2006). Multispectral data derived from Advanced Land Imager (ALI) sensors have been used to estimate the amount of CDOM present in lake waters (Kutser et al. 2005a, Kutser et al. 2005b, Cardille et al. 2013). Other studies have used satellite imagery that is specifically designed for the remote sensing of water, such as SeaWiFS. These satellites have bands in key positions for detecting subtle changes in water color, making them ideal for use in water quality studies, especially dynamic systems like coastal and oceanic regions (D'Sa and Miller 2003, Vos et al. 2003). However, sensors do not need to be designed specifically for water studies. Hyperion, for example, is used in many land-based studies and is also well designed for detecting constituents like CDOM and Chl-a (Brando and Dekker 2003, Giardino et al. 2007). However, space-based hyperspectral imagery has only been collected since the early 2000's, limiting its use for detecting historical changes in water quality parameters. Indeed, most previous studies have investigated spatial variation in water quality parameters, and few have explored the possibility of using remotely sensed imagery to assess temporal trends.

Moderate resolution imagery provides a unique opportunity in this area as they may provide long-term data needed to assess change over time. The Landsat program has one of the longest running, continuous databases of satellite imagery, having collected images since the first multispectral scanner was sent into orbit in the 1970s. It has moderate spatial, spectral, and temporal resolution of 30 meters, 7 bands, and 16 days, respectively. While Landsat is well known for its uses in land cover studies, it has also proven useful in water quality-related studies in lakes and reservoirs around the world (Carpenter and Carpenter 1983, Lathrop and Lillesand 1986, Khorram et al. 1991, Brivio et al. 2001, Giardino et al. 2001, Kloiber et al. 2002a, Kloiber et al. 2002b, Chipman et al. 2004, Hellweger et al. 2004, Wang et al. 2004, Brezonik et al. 2005, Wang et al. 2006, Olmanson et al. 2008, Hadjimitsis and Clayton 2009). For example, Kloiber et al. (2002a) and Olmanson et al. (2008) successfully used Landsat data to develop

models estimating SDD in lakes over time, resulting in R^2 ranges of 0.72 - 0.93 and 0.71 - 0.96, respectively. Models developed by Giardino et al. (2001) relating reflectance data to *in situ* data were also highly accurate, explaining a substantial fraction of the variation in SDD (R^2 = 0.85) and Chl-a, (R^2 = 0.99). Landsat ETM+, which has a slightly higher spectral resolution of 8 bands, has also been successfully used in lake studies, as well as dams, rivers, and bays (Vincent et al. 2004, Han and Jordan 2005, Alparslan et al. 2007, Kallio et al. 2008). The estimation accuracy between SDD, CDOM, and turbidity and ETM+ reflectance data in a study conducted in Finnish lakes, for instance, was R^2 = 0.78, 0.83, and 0.86, respectively (Kallio et al. 2008).

Landsat TM data has been widely used to estimate water quality indicators such as turbidity and chlorophyll-*a* in estuaries (Lavery et al. 1993, Baban 1997, Chica-Olmo et al. 2004, Carpintero et al. 2013, Mantas et al. 2013). For example, a model developed by Lavery et al. (1993) for Chl-a yielded a R^2= 0.758. If satellite data could be used to estimate SDD, Chl-a, and DOC, our ability to assess temporal changes in these constituents would be greatly expanded. Although previous research demonstrates the potential for estimating various water quality parameters using Landsat data, several issues can hinder development of robust models. Even though Landsat satellites are scheduled to collect data for a given area every 16 days, cloud cover can render a large number of images useless. Not only can this make it difficult to get a sufficiently large dataset, but it may also result in gaps in the time series that make it difficult to distinguish between noise and cyclic patterns like seasonality, which are important factors impacting some parameters like DOC. In addition, it can be difficult to collect *in situ* data at the same time as satellite overpass. Because water quality conditions can change over short periods of time, any lag between *in situ* and satellite data may introduce error and reduce the predictability of models based on that relationship. Indeed, previous research suggests that the accuracy of satellite-based estimates of water quality indicators decreases when *in situ* data and satellite images are not collected simultaneously (Lavery et al. 1993). Radiative transfer model inversions allow for the estimation of a

parameter from a satellite image without concurrent *in situ* samples and are increasingly employed (Dekker et al. 2001); however, this method requires detailed information about the scattering and absorption properties of the water body of interest which may be unavailable. Consequently, Landsat TM imagery remains an attractive potential source of information about temporal changes in water quality. A systematic evaluation of how data collection issues can affect model fit and estimation accuracy would highlight potential pitfalls associated with using satellite data for examining water quality changes.

The ability to investigate water quality at long temporal and broad spatial scales is imperative for evaluating the impact of anthropogenic influences and climate change on ecosystem structure and function (Gallegos et al. 2011). Due to its wide availability and long record, moderate resolution imagery has the potential to provide a wealth of information about the temporal and spatial variation of aquatic ecosystems. I evaluated the use of Landsat-5 TM imagery to estimate Secchi depth, chlorophyll-*a* concentration, and DOC concentration for a 248 km section of the Hudson River. My specific objectives were to: 1) construct calibration models for Landsat-5 TM reflectance values using *in situ* water quality data; 2) test the accuracy of estimates by comparing predicted and observed values from an independent dataset; and 3) explore whether factors such as input data range, model sensitivity, seasonality, and synchronicity of satellite and *in situ* data collection affect the accuracy of modeled estimates.

Chapter 2: Methods

Study Site

The Hudson River runs from Lake Tear of the Clouds in the Adirondack Mountains through southeastern New York State where it empties into the New York Harbor (Busby and Darmer 1970, Findlay 2005). The roughly 32,375 km^2 drainage basin includes numerous tributaries, the largest being the Mohawk River, and is flanked by the Catskill Mountains to the west and southwest, the Adirondacks to the north, and the Taconic Range and Green Mountains to the east (McCrone 1966). Melting snow and seasonal showers cause maximum discharge rates to occur in the spring, while minimum discharge rates are observed during the annual dry season in late summer and early fall (McCrone 1966). According to the USGS, the average annual temperature for the basin is 47 °F and the average annual precipitation ranges between 40 and 48 inches (Freeman 1991).

This study focuses on the lower, estuarine portion of the Hudson River (Fig. 1). The Hudson River Estuary constitutes the lower 248 km of the Hudson River, stretching from the Federal Dam at Troy to the Battery New York City (Busby and Darmer 1970, Freeman 1991, Findlay 2005). Beginning just downstream of the confluence with the Mohawk, the estuary flows first through farmland, and then some industrial areas before reaching the Hudson Highlands, where it passes through a deep, narrow channel with steep banks and forested mountain slopes (Freeman 1991). The river then widens near Haverstraw and narrows again before reaching the upper New York Harbor (Freeman 1991). It is a tidal estuary, undergoing a reversal of direction of flow up to four times a day (McCrone 1966, Freeman 1991). As a result, the water column is generally well mixed (Busby and Darmer 1970, Freeman 1991, Findlay 2005). A salt front is also observed as far north as Poughkeepsie, with its position depending on the total fresh-water inflow from upstream (McCrone 1966, Busby and Darmer 1970).

In Situ Data

In situ water quality data were collected between 1987 and 2008 for six cardinal stations (Findlay 2005, Larkin 2010)(Figure 1). The Kingston station was visited every two weeks during the ice-free season (April through December), while the other five were general visited in April, June, August, and October of each year (Studies 2009). Secchi depth was measured during each visit and water samples were collected from 0.5 meters below the water surface using a peristaltic pump (Studies 2009). Chlorophyll-*a* concentration was measured by filtering the water samples onto Whatman GFF filters and freezing them until methanol extraction and analysis using a Turner Fluorometer (Studies 2009). For DOC, samples were filtered through Whatman 934-AH pre-combusted filters and refrigerated until analysis with a Shimadzu high-temperature combustion organic carbon analyzer (Studies 2009). Field-filtered, sulfuric acid preserved water samples were also run using the Shimadzu analyzer and, occasionally, whole water samples were analyzed using a Shimadzu gas chromatograph for comparison with the carbon analyzer (Studies 2009).

Landsat TM 5 Data

Landsat images were downloaded from the USGS Earth Explorer website, omitting those with greater than 80% cloud cover. Each pixel is 30 x 30 m in size and all images are spatially referenced using UTM Zone 18N WGS 1984. Because a majority of the images were not taken on the exact same day that the *in situ* data were collected, a seven day window around each date was used to ensure a sufficient number of images. Although this may introduce some error in the results, other studies in which satellite and field data were paired agreed that while a one day difference yields the best calibrations, it is acceptable to increase this window when data are sparse (Kloiber et al. 2002b, Sawaya et al. 2003, Olmanson et al. 2008).

Bands 1 - 4 of each Landsat image were layer stacked to create a single image. Band 1 spans the wavelength range of 0.45-0.515 um in the blue portion of the electromagnetic spectrum, Band 2 the

green portion from 0.525-0.605 nm, Band 3 the red portion from 0.63-0.69 nm, and Band 4 the near infrared from 0.75-0.9 nm. These bands were chosen because previous studies have found correlations between DOC, Secchi depth, and chlorophyll-*a* concentration and these bands (Harrington Jr et al. 1992, Baban 1993, Lavery et al. 1993, Pattiaratchi et al. 1994, Allee and Johnson 1999, Giardino et al. 2001). These images were atmospherically and radiometrically corrected using the Atmospheric Correction and Haze Reduction (ATCOR) extension for the Earth Resources Data Analysis System (ERDAS). ATCOR was developed specifically to account for about 80% of typical conditions that are observed, taking into account the influence of the atmosphere, solar illumination, sensor viewing geometry, terrain geometry, and sensor attributes (Richter 2010). While ATCOR is not specifically tailored to a region or time an image was taken, it has been successfully used to correct images in the past (Richter 1996, 1997, Hadjimitsis et al. 2004). All image analyses were performed using ERDAS Imagine 2010 and ArcGIS 10.0.

One subset image from each of 167 Landsat images was paired with a corresponding subset from a reference image, which was taken approximately midway through the time span. The subsets averaged ca. 400 x 400 pixels in size and were arbitrarily chosen as the best representatives of each scene; that is, with minimal cloud cover and a range of pixels that were unlikely to have changed over time (e.g. bare ground, paved areas, etc.). To normalize the images over time, I applied iMad and Radcal programs to the subset images for the reference image and image of interest (Canty and Nielsen 2008). iMad uses iteratively reweighted multivariate alteration detection to determine pixels that have not changed over time (Nielsen 2007, Canty and Nielsen 2008), and Radcal radiometrically corrects the full original image based on the unchanged pixels identified (Canty and Nielsen 2008). The success of this correction was determined by looking at the regression lines comparing the predicted versus actual pixel values for each band (Fig. 2). Images that showed a "gunshot" correlation with a R^2 less than 0.9 for any of the four bands were deemed unsuccessful and thrown out, while those showing a strong correlation, with R^2 higher than 0.9, for all four bands were used in subsequent analyses.

Statistical Analyses

The pixel values for each Cardinal station were collected for Band 1 (blue), Band 2 (green), Band 3 (red), and Band 4 (near-infrared) of each corrected image taken between 1988 and 2004. The four band values and all possible ratios of these bands were then pooled together and regressed against empirical water quality data. Because dividing one band by another can often serve to normalize the brightness in band of interest, these ratios can be useful in explaining the variability in the *in situ* data (Matthews 2011). Although certain bands and band ratios have previously been associated with water quality parameters, I considered all possible bands and band combinations equally. Variables were transformed as needed to meet regression assumptions. Specifically, I applied a log transformation to Chl-a to account for the non-linear relationship between this constituent and reflectance (Lavery et al. 1993). Outliers were identified by calculating Cook's D values, and those observations that had a value of > 2 were examined and removed if deemed to have a significant influence on the data (Stevens 1984). I used an information theoretic approach to determine all possible models that could describe the relationship between the reflectance data and water quality indicators. Corrected Akaike information criterion (AIC_C) and subsequent delta AIC_C (Δ_i) values, which are a measure of support for each model relative to the best model, were calculated using these values. The best subset of models for each water quality parameter was selected based on the criteria that any model with a delta AIC_C > 2 became obsolete, and model probabilities (w_i) for this subset were calculated (Burnham and Anderson 2002). I computed an averaged model for each water quality parameter by weighting the model coefficients for the subset using w_i (Gibson et al. 2004) and used the averaged models and a set of Landsat images taken between 2005 – 2008 to map DOC, SDD, and Chl-a for the estuary. To test the accuracy of these estimates, I compared the estimated values with observed values from an independent data set for corresponding locations and dates by calculating Pearson product-moment correlations, as well as the

root mean squared error (RMSE), which is a standard measure of error between predicted and observed results calculated in the units of the data of interest.

To evaluate whether certain factors influence the accuracy of the models, I carried out several additional analyses. To determine whether the ranges of data values for the validation data sets generally fell within those of the training data sets, I generated box and whisker plots to visually compare the range of estimated and observed values. Overlay plots showing the estimated and observed data over time were created to assess the overall sensitivity of the models as well as to look for indicators of seasonality. I also evaluated whether asynchrony between the satellite overpass time and *in situ* data collection affected accuracy by comparing the correlation between estimated and observed values for a subset of data in which the difference in overpass and collection time was ≤ 1 day.

Chapter 3: Results

The *in situ* water quality dataset consisted of 158 observations for SDD and DOC, and 153 for Chl-a (Table 1). Both SDD and Chl-a had wide ranges of 180 cm and 85.09 ug/L, respectively (Table 1). The range of DOC values was narrower, spanning only 6.58 mg/L (Table 1).

Of the 242 possible models, 68 were deemed to be the best subset based on Δ_i for SDD (Appendix A). The best model was comprised of B1, B3, B1/B3, B2/B3, and B2/B4, and had a $w_i = 0.028$, with the w_i of the next ten models all falling within 0.01 of this value (Eq. 1, Table 2, Appendix A). The fact that no w_i value was significantly higher than the rest strongly supports the decision to average all models included in the best subset. The averaged model for SDD had 15 variables, including B1 through B4 and their various ratios (Eq. 2, Appendix A).

(Eq. 1) $$SDD = 119.74 + 1.25 * B1 - 3.05 * B3 + 5.25\left(\frac{B1}{B3}\right) - 2.41\left(\frac{B2}{B3}\right) - 0.19\left(\frac{B2}{B4}\right)$$

(Eq. 2) $$SDD = 129.25 + 0.72 * B1 - 0.98 * B2 - 1.73 * B3 + 0.01 * B4 + 8.36\left(\frac{B1}{B2}\right) + 5.18\left(\frac{B1}{B3}\right) - 0.07\left(\frac{B1}{B4}\right) - 2.37\left(\frac{B2}{B3}\right) - 0.41\left(\frac{B2}{B4}\right) + 0.42\left(\frac{B3}{B4}\right) - 0.02\left(\frac{B2}{B1}\right) - 0.59\left(\frac{B3}{B1}\right) - 0.03\left(\frac{B3}{B2}\right) - 13.55\left(\frac{B4}{B2}\right) + 0.12\left(\frac{B4}{B3}\right)$$

For log(Chl-a), the best subset consisted of 12 models (Appendix B). The best model consisted of only B2, and had a $w_i = 0.18$ (Eq. 3, Table 3, Appendix B). Though the difference between the top two w_i was larger than for SDD at 0.08, it was small enough to justify model averaging (Table 3, Appendix B). The resulting averaged model had 11 variables, including B1 through B4 and their various ratios (Eq. 4, Appendix B).

(Eq. 3) $$\log(Chla) = 0.79 - 0.0084 * B2$$

(Eq. 4) $$log(Chla) = 0.78 + 8.76E^{-04} * B1 - 8.90E^{-03} * B2 + 1.51E^{-04} * B3 + 1.31E^{-04} * B4 - 7.40E^{-04}\left(\frac{B1}{B3}\right) - 6.14E^{-05}\left(\frac{B1}{B4}\right) - 6.86E^{-04}\left(\frac{B2}{B3}\right) - 2.33E^{-05}\left(\frac{B2}{B4}\right) - 2.53E^{-05}\left(\frac{B3}{B4}\right) - 3.32E^{-04}\left(\frac{B2}{B1}\right) + 5.85E^{-04}\left(\frac{B3}{B1}\right)$$

The best subset of models for DOC consisted of 226 models (Appendix C). The best model contained B1, B2, B4, and B2/B4, and had a w_i = 0.0086 (Eq. 5, Table 4, Appendix C). The small w_i coupled with the fact that the difference between the w_i of most of the models included in the subset was ~0.001 strongly supported model averaging (Table 4, Appendix C). The result was an averaged model that included every band and band ratio, with 16 total variables (Eq. 6, Appendix C).

(Eq. 5) $$DOC = 4.77 - 0.061 * B1 + 0.067 * B2 - 0.016 * B4 - 0.0088(\frac{B2}{B4})$$

(Eq. 6) $$DOC = 4.93 - 1.03E^{-02} * B1 + 1.60E^{-02} * B2 + 4.32E^{-03} * B3 - 1.41E^{-02} * B4 - 1.65E^{-01}\left(\frac{B1}{B2}\right) - 2.43E^{-02}\left(\frac{B1}{B3}\right) - 8.69E^{-03}\left(\frac{B1}{B4}\right) - 1.82E^{-03}\left(\frac{B2}{B3}\right) - 6.83E^{-03}\left(\frac{B2}{B4}\right) + 9.67E^{-03}\left(\frac{B3}{B4}\right) + 1.28E^{-02}\left(\frac{B2}{B1}\right) + 6.89E^{-02}\left(\frac{B3}{B1}\right) - 1.39E^{-04}\left(\frac{B4}{B1}\right) - 4.91E^{-03}\left(\frac{B3}{B2}\right) + 6.98E^{-03}\left(\frac{B4}{B2}\right) - 7.84E^{-03}(\frac{B4}{B3})$$

For the averaged and best (i.e., lowest AIC_c) models, the strength of the correlation between estimated and observed values of water quality varied by constituent. Secchi depth showed the strongest relationship (r= 0.62, P= <0.0001, Fig. 5a), followed by Chl-a (r = 0.31, P= 0.027, Fig. 5b), and DOC (r = 0.26, P=0.066, Fig. 5c) for the averaged models. The RMSE was 20.24 cm for SDD, 0.49 ug/L for Chl-a, and 0.24 mg/L for DOC. Using the best model yielded similar results, with SDD having the highest correlation (r= 0.67, P= <0.0001, Fig. 6a), Chl-a the second highest (r = 0.31, P= 0.027, Fig. 6b), and DOC the lowest (r= 0.22, P= 0.11, Fig. 6c). The RMSE was 14.85 cm for SDD, 0.52 ug/L for Chl-a, and 0.30 mg/L for DOC.

Maps of estimated water quality indicators demonstrated both spatial and temporal variability. SDD values appeared to be slightly higher in the upper half of the estuary, falling within 150-200 cm, than in the lower half where they were 101-150 cm (Fig. 3). Similarly, Chl-a displayed higher values, around 0.81-0.9 ug/L, in the upper reach and lower values, around 0.51-0.7 ug/L, downstream (Fig. 4). Temporally, Chl-a showed only a slight decrease in 2006, with concentrations in the lower reach falling to 0.51-0.6 ug/L, while SDD remained consistent throughout (Fig. 4, Fig. 3). Due to the low accuracy of DOC estimates, this variable was not mapped.

Boxplots showed no evidence that the range of values for SDD and DOC for the validation data sets fell outside that of the training data sets (Fig. 7a, Fig. 7c). For log(Chl-a), however, the training dataset is well within the range of the validation dataset (Fig. 7b). The overlay plot of estimated and observed data over time for log(Chl-a) showed a similar pattern, in that the range of estimated values was much narrower than that of the observed values (Fig. 8b). Likewise, the overlay plots for SDD showed that the estimated and observed values had similar ranges over time (Fig. 8a). Although the boxplot for DOC indicated that the range of values in the training data to encompassed the range of values in the validation dataset, estimated values did not track observed values and their range was much narrower than for the observed values (Fig. 8c). Notably, observed values of DOC show a seasonal pattern that is not apparent in the estimated data (Fig. 8). Finally, excluding data where the difference in collection day was ≤ 1 resulted in a higher correlation between estimated and observed values for SDD ($r= 0.72$, $P= 0.0005$, Fig. 9a). However, it did not strengthen the correlation between estimated and observed data for log(Chl-a) ($r= 0.20$, $P= 0.43$, Fig. 9b) or DOC ($r= 0.045$, $P= 0.85$, Fig. 9c).

Chapter 4: Discussion

Given the potential of moderate resolution imagery for use in estuarine water quality studies, I sought to determine whether Landsat imagery could be used to predict water quality characteristics in the Hudson River estuary, as well as what factors may influence the accuracy of estimates derived from Landsat TM imagery. I find that Landsat imagery can be used to predict Secchi depth and chlorophyll-a concentration in an estuarine system with moderate to high accuracy. Spatial patterns derived from these models suggest that SDD and Chl-a concentration decreased with increasing distance downstream; however, these spatial gradients became less apparent over time. Further analysis suggests that lack of synchrony between satellite overpass and collection of *in situ* training data may reduce the fit of the calibration model and lower the accuracy of estimates.

There was general agreement between the variables deemed most correlated with SDD, Chl-a and DOC by the AICc analysis and those found in the literature, providing evidence that AICc model selection was successful in identifying variables known to be associated with the water quality variables of interest. B2 was included in all but one model in the best subset for Chl-a, which was also found to be important by Allee and Johnson (1999) and Lavery et al. (1993). As B2 includes the green wavelength region of the visible spectrum, it is logical that this would be the most common band associated with Chl-a. Similar to others, I found that B1, B3, and associated ratios were important for predicting SDD, with B1/B3 occurring in all models included in the best subset (Pattiaratchi et al. 1994, Allee and Johnson 1999, Kloiber et al. 2002b, Chipman et al. 2004, Olmanson et al. 2008). The short wavelengths of B1 fall in the blue region of the visible spectrum, making it well suited to penetrate the water column and detect the presence sediments or other particulates. B3, the red band, absorbs strongly with the presence of chlorophyll and has been found to be correlated with suspended sediment concentration and turbidity, which greatly impacts water transparency and, thus, SDD (Sváb et al. 2005, Bustamante et al. 2009). In agreement with Arenz et al. (1996) and Hirtle and Rencz (2003), B2, B3, and B4 all occurred

frequently in the best subset of models for DOC, with B4, the near-infrared band, occurring in nearly all of them. DOC generally absorbs across the spectrum, though not at wavelengths above 650 nm. This makes B4's presence a bit surprising, since it spans 760-900 nm, but its utility in predicting DOC concentration may lay in an interaction with suspended sediments that is not yet well understood (Arenz et al. 1996, Hirtle and Rencz 2003).

In comparing the best and averaged models, the relatively low w_i and negligible difference between the w_i of the best model and those for the rest of the models in the best subsets provided a strong argument for model averaging. However, the averaged models included noticeably more variables than the best model, raising the question of whether model averaging yielded better performing models. Evaluating the agreement between estimated and independently observed values of Secchi depth, I found that the RMSE was lower for the best model, at 14.85 cm. This suggests the best model performed slightly better than the averaged model. Comparison of RMSE for Chl-a and DOC, on the other hand, showed very little difference indicating that the inclusion of more variables did not have a strong influence on estimation accuracy. These findings suggest that model averaging did not necessarily improve model performance in this case. However, additional research is needed to determine if model averaging yields better performing models under other conditions.

Estimation accuracy was also evaluated by examining the correlation between predicted and observed values for a validation dataset. The high correlation between estimated and observed Secchi depth is consistent with the results of other studies. Being an indicator of water clarity, Secchi depth is nearly a direct measure of water reflectance and thus it is expected that changes in this parameter are apparent in the satellite imagery. Several previous studies have found highly predictive models with R-square values above 0.7 (Baban 1993, Lavery et al. 1993, Pattiaratchi et al. 1994, Allee and Johnson 1999, Giardino et al. 2001). However, most of these studies were done on bodies of water such as lakes

or reservoirs, which behave much differently than tidal estuaries (Baban 1993, Allee and Johnson 1999, Giardino et al. 2001). For example, when correlating SDD and Chl-a concentrations to reflectance data in the New York Harbor, Hellweger et al. (2004) highlighted the importance of minimizing the time difference between ground and satellite observations in tidal systems because factors like short-term meteorological events and tidal velocities can result in significant changes in water quality. In addition, most of these studies did not use data that spanned more than five years, lessening the amount of noise that longer-term datasets are subject to and potentially limiting the extent to which they may extrapolate their results across time (Khorram et al. 1991, Lavery et al. 1993, Pattiaratchi et al. 1994, Giardino et al. 2001).

The correlation between estimated and observed Chl-a was lower than has been achieved in other studies (Lathrop and Lillesand 1986, Brivio et al. 2001, Giardino et al. 2001, Brezonik et al. 2005, Wang et al. 2006). However, almost all of these studies were conducted on lakes which behave very differently than estuaries, being more stagnant and not as influenced by factors like salt fronts (Baban 1993, Giardino et al. 2001, Chen et al. 2008). The Hudson also experiences tides and has a well-mixed water column, both of which can result in lower Chl-a levels, which are more difficult to detect (Monbet 1992). For example, under lower Chl-a concentrations, the signal for Chl-a may be swamped by the signal from a more dominant, non-chlorophyllous constituent, such as suspended sediments (Sathyendranath et al. 1989, Ekstrand 1992).

DOC yielded the weakest correlation between predicted and observed values. Although some studies have successfully estimated DOC using predictive models (Vertucci and Likens 1989, Arenz et al. 1996, Kondratyev et al. 1998), a majority concluded that sensors with radiometric resolutions less than 16-bit are unable to provide accurate estimations of DOC (Kutser et al. 2005a, Kutser et al. 2005b, Kallio et al. 2008, Kutser et al. 2009). This can be explained by the fact that DOC itself is not optically active but

rather it is detected by a lack of signal in the blue visible spectrum, and energy absorption due to DOC is often masked by reflectance of Chl-a and other particulates in the water column (Arenz et al. 1996). Consequently, models derived from moderate resolution imagery lack the sensitivity necessary to detect small changes in DOC and detection is most successful when using sensors with higher spatial and spectral resolution (Gons 1999, Doxaran et al. 2002, Doxaran et al. 2003, Doxaran et al. 2006).

Spatio-temporal patterns

There were clear patterns in the spatial distribution of Chl-a and Secchi depth. Chl-a concentration was higher in the upper, narrower half of the estuary than the lower, wider half. This may indicate a higher abundance of phytoplankton or other primary producers that contain chlorophyll. Consistent with this pattern, I found that SDD was lower in the upper reach, suggesting reduced water clarity. The influence of tides and the moving salt front, both of which can impact turbidity and Chl-a, are more pronounced downstream. For instance, a study by Wurtsbaugh and Berry (1990) found that abnormally low salinity levels in the Great Salt Lake in Utah caused a shift in the macrozooplankton community that resulted in reduced grazing pressure on the algal community and thus higher Chl-a concentrations and low SDD. Thus, it is possible that the varying salinity levels throughout the reach of the Hudson are having similar cascading effects. However, the degree to which salinity may be affecting the results is difficult to ascertain due not only to its varying position, but also its wedge shape brought on by the difference in densities of fresh and saline waters. Additional research is needed to determine the effect of the position of this front on the spatial distribution of SDD and Chl-a in the Hudson.

Temporal patterns in Chl-a and SDD were less pronounced. Over time, Chl-a only slightly decreased one year and SDD appeared to remain fairly constant. These constituents are subject to seasonal variation, with spring thaw resulting in an influx of nutrients and sediments that would impact both SDD and Chl-a concentration. However, because I mapped values for the same month across four

years, seasonal fluctuations may not be evident. Focusing on other time intervals may be more informative for monitoring temporal patterns in SDD and Chl-a.

Factors affecting estimation accuracy

In addition to parameter-specific explanations, I determined whether other factors could account for differences in the models' predictive power. I found little evidence that the range of the training data was too narrow to allow for a successful extrapolation of water quality indicators. For SDD and DOC, the ranges of values for the validation data sets generally fall within that of the training data sets, which suggests that extrapolating is statistically valid. For log(Chl-a), however, the training dataset is well within the validation dataset, which may explain why the model for Chl-a was less robust and yielded less accurate estimates of Chl-a.

We fit linear models to the data, but seasonal trends may warrant fitting nonlinear models to the data. Temporal patterns are evident in the overlay plots and are consistent with major shifts in weather in the region. The spring thaw of snow along the northern portion of the Hudson brings a large influx of materials like DOC and suspended sediments, which impact SDD (McCrone 1966, Busby and Darmer 1970). Nutrient inputs during the warm summer months can cause increases in phytoplankton and thus Chl-a (Busby and Darmer 1970). Future research should investigate whether fitting a model that accounts for seasonal patterns explains more variation in DOC and allows for greater estimation accuracy. In the current study, this approach was not feasible because there were too few dates where *in situ* and satellite data overlapped.

The difference in dates between sample and satellite images can also affect estimation accuracy. Previous studies that have succeeded in producing highly accurate maps of the distributions of SDD and Chl-a, as well as other water quality parameters such as temperature, salinity, and turbidity, constructed models based on satellite data that was collected contemporaneously with *in situ* data

(Lathrop and Lillesand 1986, Khorram et al. 1991, Lathrop 1992, Lavery et al. 1993, Wang et al. 2004). In this study, a seven day window was used in order to ensure a sufficient number of samples to build the models, as well as to help dampen signal noise. During this time, extreme weather events and large influxes of suspended sediments may have altered water quality and associated patterns of energy reflectance. This in turn would reduce model fit and estimation accuracy. Indeed, I found that the correlation between predicted and observed values improved for SDD when I removed values where the difference in collection day for the satellite and *in situ* data was > 1 day (Fig. 9). This supports the hypothesis that the estimation accuracy is higher when satellite and *in situ* data collection are synchronously. Likewise, the accuracy of log(Chl-a) estimates improved when I excluded values where the satellite images were collected ≤ 2 days from the *in situ* data, but declined once I excluded those with a difference of ≤ 1 day. This may indicate that Chl-a concentrations do not change significantly over short periods of time, meaning that collecting *in situ* data and satellite data simultaneously may not be absolutely necessary. In contrast, the correlation between estimated and observed values of DOC did not improve when asynchronous data were excluded. Like Chl-a, it may be that simultaneous collection times are less important for predicting DOC. However, because DOC is a notoriously difficult constituent to detect, any difference in collection time may amplify errors, especially in dynamic systems like estuaries (Matthews 2011). Nevertheless, these results should be interpreted cautiously as excluding the non-synchronous data reduced the sample size from 52 to 19 for SDD and DOC, and 51 to 19 for Chl-a, and were less significant. Hence, the improved correlation or lack thereof between predicted and observed values may be an artifact of reduced sample size.

Mismatches between the spatial resolution of remote sensing and *in situ* data can also affect estimation accuracy. In the present study, Landsat reflectance data was paired with one *in situ* value for TOC, SDD, and Chl-a. I assumed each of these values uniformly represented a 30x30 m area; however, this may not have been the case. When sampling estuaries for image calibration, it may be necessary to

sample water quality at multiple points within an area and average them together to characterize that area. Khorram et al. (1991), for example, collected 42 water quality samples within an hour of the Landsat satellite overpass and produced predictive models with R^2= 0.83 and 0.84 for SDD and Chl-a, respectively. Lavery et al. (1993) also developed a highly significant, predictive algorithm for SDD (R^2= 0.75), as well as for pigment concentration (R^2= 0.76) and salinity (R^2= 0.78) based on field data collected at the same time as satellite overpass. Coupled with the wide bands and low signal-to-noise ratio of Landsat, limited *in situ* data may hinder development of robust calibration models. A much larger dataset may be needed to improve calibration models.

In addition, the corrections applied to the Landsat images may have introduced noise. Atmospheric corrections are important as they account for factors that can alter the reflectance value and result in the drawing of erroneous conclusions. However, although the correction methods used in this study are well accepted, they were somewhat generic in that they did not account for area specific atmospheric conditions, like atmospheric thickness or gas content. Giardino et al. (2001), for example, used atmosphere-specific parameters to correct the Landsat images used to build their models and were very successful in predicting SDD and Chl-a. They also applied the same correction throughout an entire image, assuming atmospheric conditions were uniform throughout. It is possible that by ignoring these factors, correcting the image could cause errors. This can be especially true when trying to remotely sense a constituent like DOC, which is detected by a lack of signal in the blue band. Should the image be overcorrected, the DOC signal could be masked or enhanced, resulting in improper detection.

When both atmospherically correcting the images and building the statistical models, we assumed the water and atmosphere maintained uniform conditions throughout each image when this is not likely the case (Matthews 2011). The Hudson River Estuary spans a large area that can experience different conditions simultaneously. This was evident in my observation of images where certain areas

had cloud cover while others did not, as well as the fact that the physical characteristics of the estuary vary greatly. For example, a portion of the Hudson passes through a narrow valley in the Catskill Mountains, which affects the depth and width of the water body, as well as the velocity and roughness of the water's surface. The mouth of the estuary empties into the New York Harbor, where the estuary is both wider and deeper, resembling conditions encountered in lakes. Tides and a moving salt front also impact the lower half of the estuary to varying degrees (McCrone 1966, Busby and Darmer 1970). To a certain extent, the models generated should be robust against these limitations. There have been a number of cases where combining all data for an entire water body dampened the noise that considering each sample site individually can create, resulting in highly predictive models (Matthews 2011). However, as the assumption of uniform atmospheric conditions breaks down, so increases the relative errors in parameter estimates (Matthews 2011). This is especially true when looking across time (Matthews 2011).

Lastly, it is possible that not enough details were accounted for in the models or atmospheric corrections. We used an empirical approach, regressing satellite reflectance data against *in situ* data collected as close to concurrently as possible. While this is a well-accepted method, given the complexities associated with the remote sensing of water, there is a strong argument for using a semi-analytical approach that employs bio-optical models to establish a relationship between satellite data and water quality parameters (Ma et al. 2006, Matthews 2011). These models incorporate information about the inherent optical properties (IOPs) and apparent optical properties (AOPs) of water as a function of specific total absorption and backscattering values, with different models applying to different bodies of water (Ma et al. 2006). The result is a much more thorough accounting of what is occurring not only at the surface of the water, but also within the water column down to the stream bed. Although the calibration models constructed in this study yielded reasonably accurate estimates for SDD and Chl-a, accuracy may be enhanced if optical properties are accounted for. Nonetheless, because

this study was mainly interested in what basic relationship could be established between reflectance data and water quality parameters for a specific region, the empirical method employed was appropriate.

Chapter 5: Conclusion

Using AIC analysis, I built averaged models based on reflectance data from Landsat TM and *in situ* data for SDD, Chl-a, and DOC collected between 1989 and 2004. Models for SDD and Chl-a yielded accurate estimates when tested against an independent dataset. The success of these models suggests a strong potential for Landsat imagery to be used to monitor SDD and possibly Chl-a for this area. DOC, however, may require a higher resolution sensor or much more synchronous satellite and *in situ* data collection dates for improved detection accuracy.

Among the caveats of this study is the scope of applicability. Although the models for SDD and Chl-a may seem relatively robust, it is unlikely they could be used in a different estuary to accurately characterize water quality because differences in scattering within the water column may create error that could detract from the models' ability to make accurate estimations. A bio-optical model together with *in situ* and reflectance data may be needed to create calibration models that that allow for accurate estimation of water quality at the global scale (Ma et al. 2006). Studies using this kind of satellite data may also be limited in terms of sample size due to factors like cloud cover and collection date overlap. In this study, these factors reduced a 20 year dataset with hundreds of images and *in situ* data points to an n of only 152. Although this is still a relatively large number of images, the gaps and inconsistent timing of the data may have hindered our ability to detect temporal trends that were less pronounced. Hence, as concluded in Lavery et al. (1993), this method of monitoring water quality may only be feasible as a supplementary source of information to other means.

Even so, this study accomplished an important goal in identifying a feasible means to detect water quality parameters across both time and space. It is this kind of knowledge that will enable us to better understand the state of our water bodies which, as our ecosystems continue to be altered by

both anthropogenic activities, will become increasingly important to managing and preserving these aquatic systems in the future.

Chapter 6: Tables

Table 1. Summary statistics of *in situ* data for SDD and DOC.

	Secchi Depth (cm)	Chl-a (ug/L)	DOC (mg/L)
Average	95.60	7.20	5.04
Standard Deviation	37.82	9.37	1.30
Max	200	85.83	7.70
Min	20	0.74	1.12
N	158	153	158

Table 2. Model characteristics for the top five models in the best subset describing Secchi depth in the Hudson River.

Model	K	AIC	AICc	Delta AIC_C (Δ_i)	Relative Likelihood	Akaike (w_i)	Model Variables
1	5	1114.016	1114.4	0	1	0.027916	B1 B3 B1_B3 B2_B3 B2_B4
2	5	1114.178	1114.562	0.1619	0.92224	0.025745	B1 B3 B1_B3 B1_B4 B2_B3
3	5	1114.188	1114.573	0.1722	0.917502	0.025613	B1 B2 B1_B3 B2_B3 B4_B2
4	5	1114.207	1114.592	0.1915	0.908691	0.025367	B2 B1_B2 B1_B3 B2_B3 B4_B2
5	6	1114.117	1114.658	0.25802	0.878965	0.024537	B3 B1_B2 B1_B3 B2_B3 B2_B4 B4_B2

Table 3. Model characteristics for the top five models in the best subset describing Chl-a concentration in the Hudson River.

Model	K	AIC	AICc	Delta AIC_C (Δ_i)	Relative Likelihood	Akaike (w_i)	Model Variables
1	1	702.1344	702.1602	0	1	0.180478	B2
2	1	703.3293	703.3551	1.1949	0.550213	0.099301	B3
3	2	703.7232	703.8011	1.640916	0.44023	0.079452	B2 B2_B3
4	2	703.7594	703.8373	1.677116	0.432334	0.078027	B1 B2
5	2	703.8846	703.9625	1.802316	0.406099	0.073292	B2 B2_B4

Table 4. Model characteristics for the top five models in the best subset describing DOC in the Hudson River.

Model	K	AIC	AICc	Delta AICc (Δ_i)	Relative Likelihood	Akaike (w_i)	Model Variables
1	4	88.4978	88.75258	0	1	0.008595	B1 B2 B4 B2_B4
3	4	88.6082	88.86298	0.1104	0.946296	0.008133	B4 B1_B2 B1_B3 B2_B4
4	4	88.6564	88.91118	0.1586	0.923763	0.00794	B1 B2 B4 B1_B4
2	2	88.8514	88.92687	0.174295	0.916542	0.007878	B4 B3_B1
6	5	88.5727	88.95732	0.204738	0.902696	0.007759	B1 B2 B4 B1_B3 B2_B4

Chapter 7: Figures

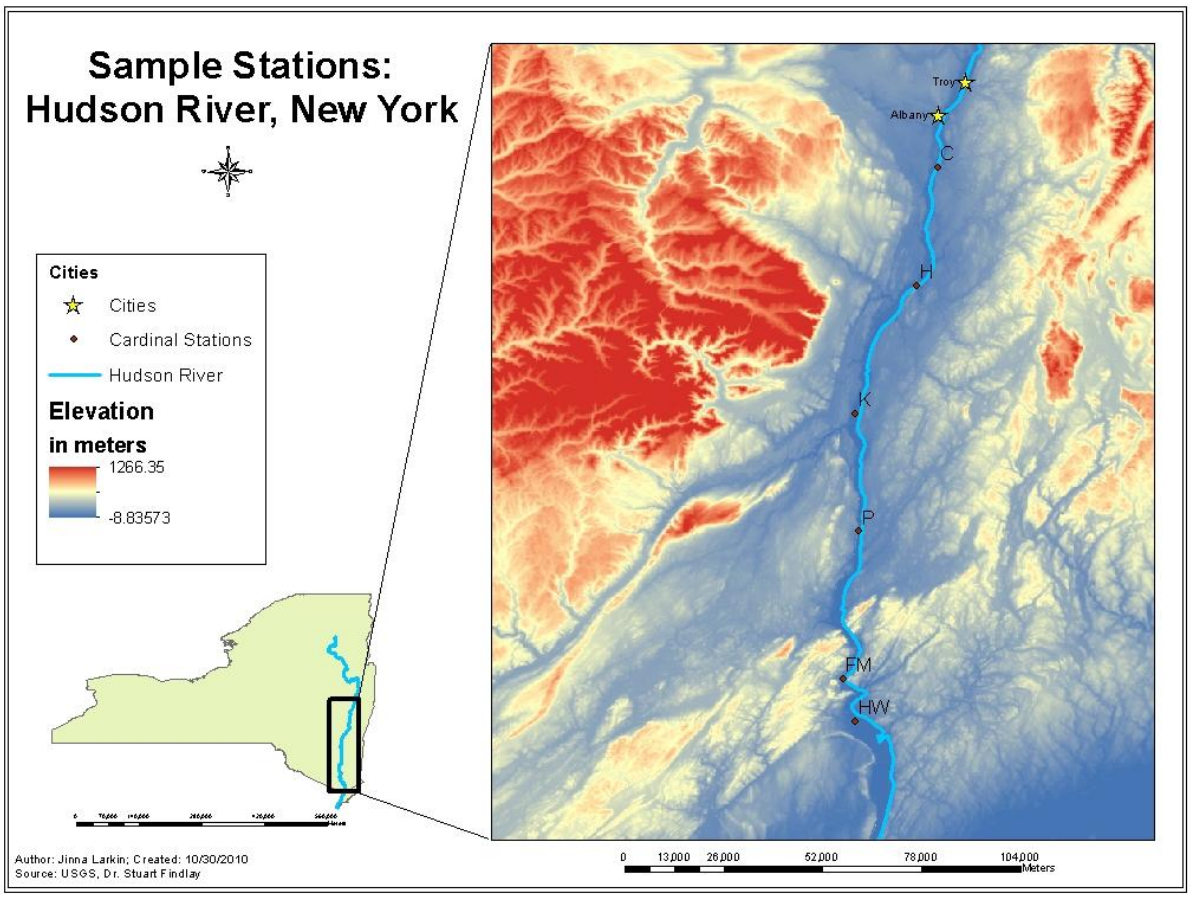

Figure 1. Map of the Hudson River showing the locations of the six Cardinal stations where *in situ* data was collected.

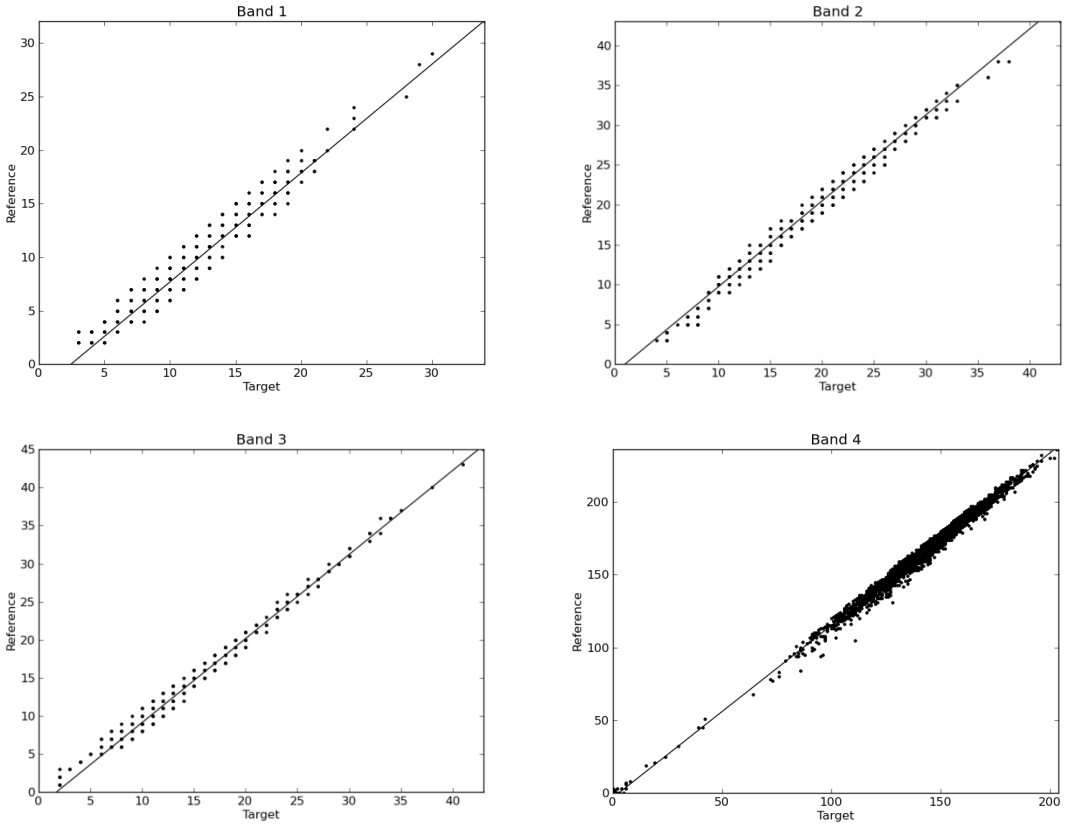

Figure 2: Correlation between no-change pixel values for bands 1-4 from a reference image and a Landsat-5 TM image taken on August 19, 2001, indicating a successful iMad/Radcal procedure.

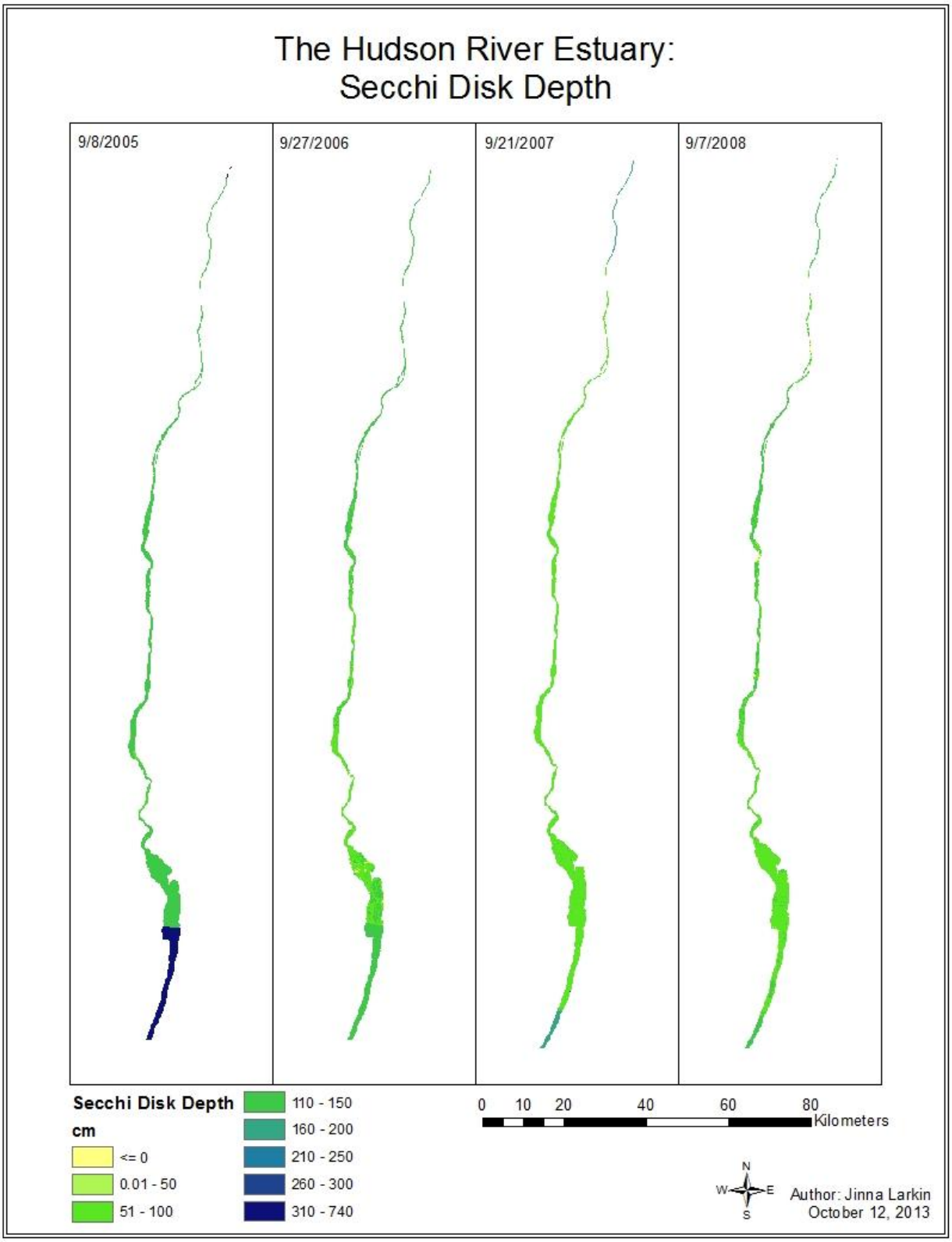

Figure 3: Predictive maps of SDD derived using model-averaged parameter estimates and images taken in September between 2005 and 2008.

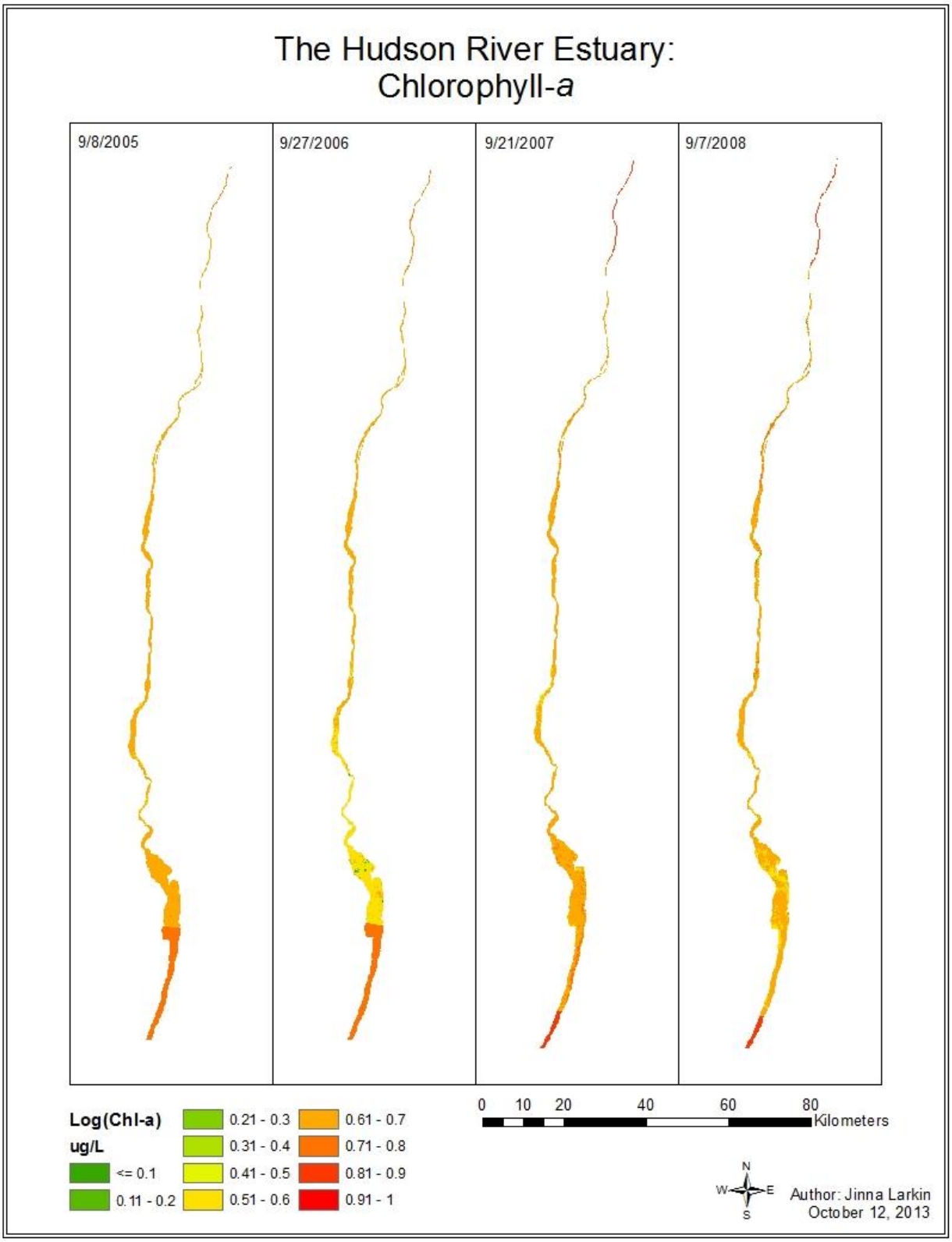

Figure 4: Predictive maps of log(Chl-a) derived using model-averaged parameter estimates and images taken in September between 2005 and 2008.

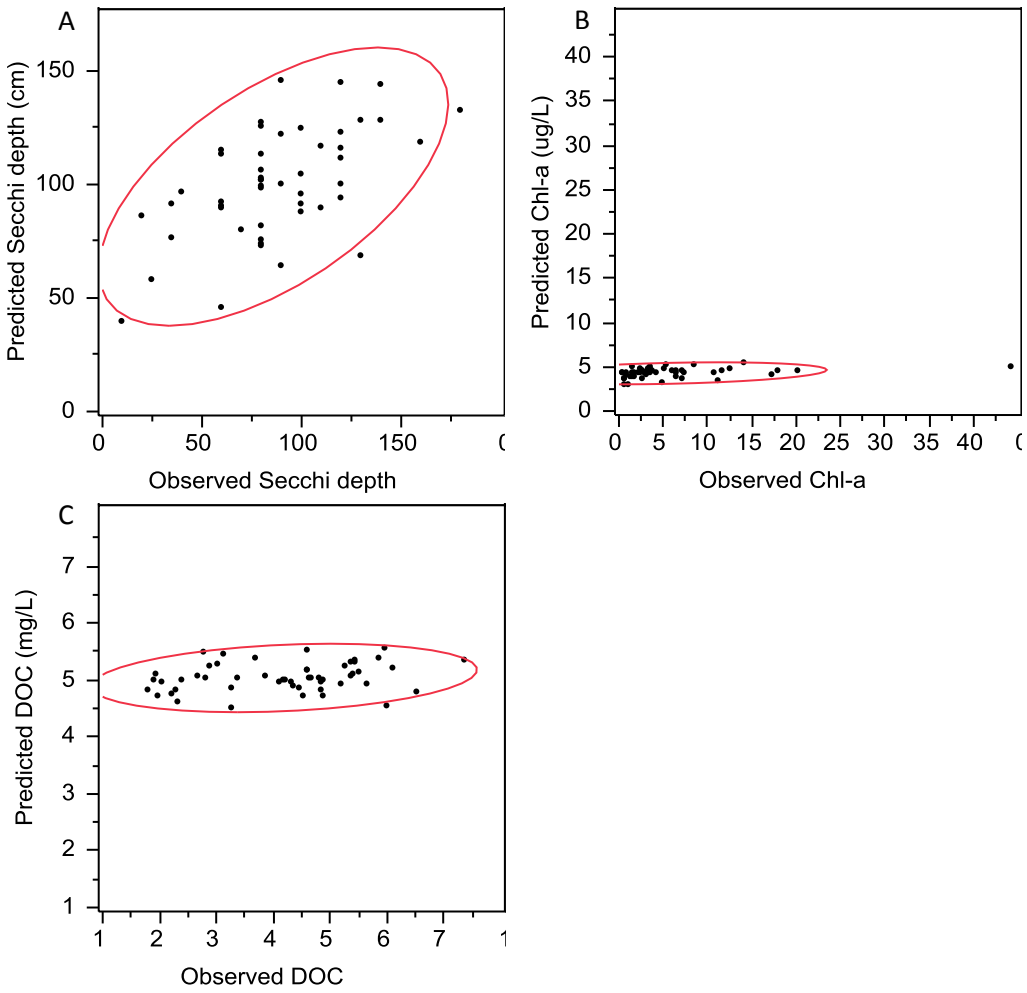

Figure 5: Predicted versus observed values using the averaged model for Secchi depth (r = 0.62, P= <0.0001) (A); Chl-a (r = 0.31, P= 0.027) (B); and DOC (r = 0.26, P= 0.066) (C). *In situ* data are from an independent dataset that was not used to generate the calibration models. Images used for prediction were selected to minimize the time between satellite overpass and *in situ* sampling (>= 7 days of *in situ* data collection).

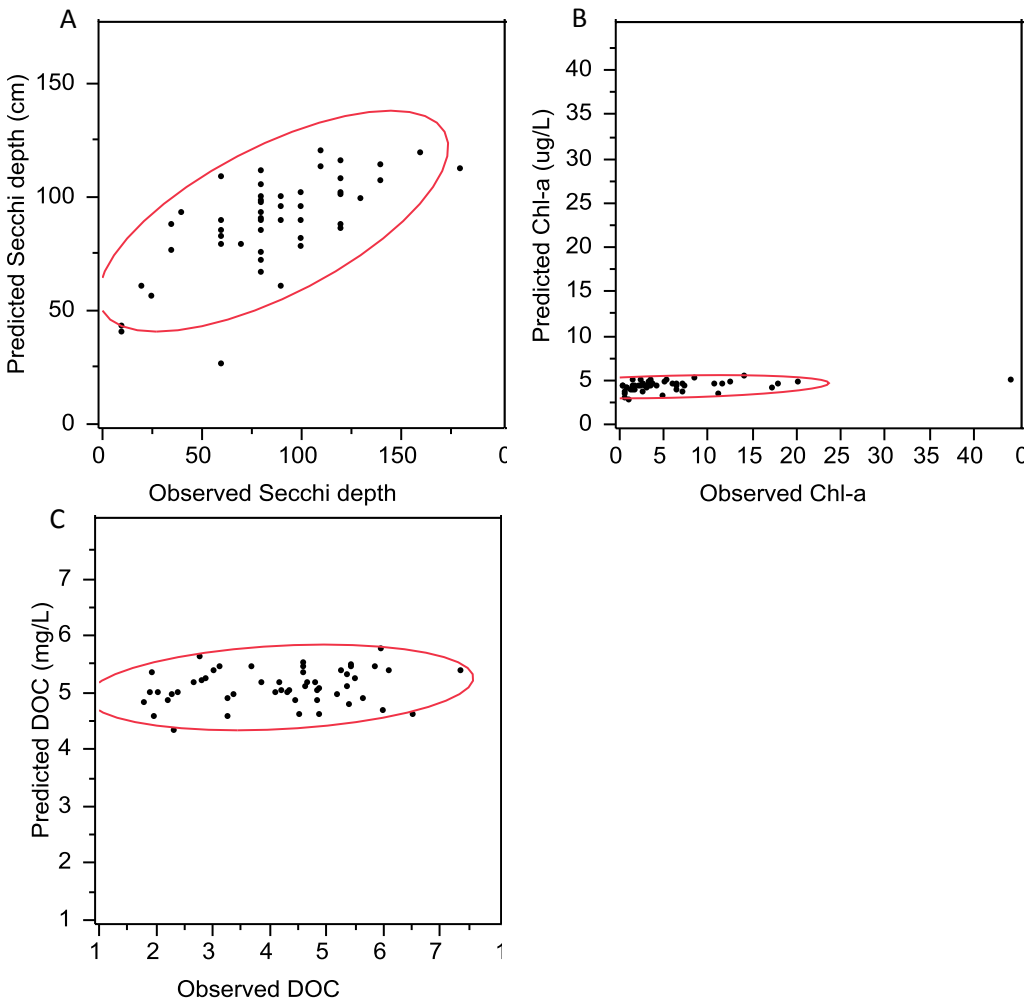

Figure 6: Predicted versus observed values using the best model for Secchi depth (r = 0.67, P= <0.0001) (A); Chl-a (r = 0.31, P= 0.027) (B); and DOC (r = 0.22, P= 0.11) (C). *In situ* data are from an independent dataset that was not used to generate the calibration models. Images used for prediction were selected to minimize the time between satellite overpass and *in situ* sampling (>= 7 days of *in situ* data collection).

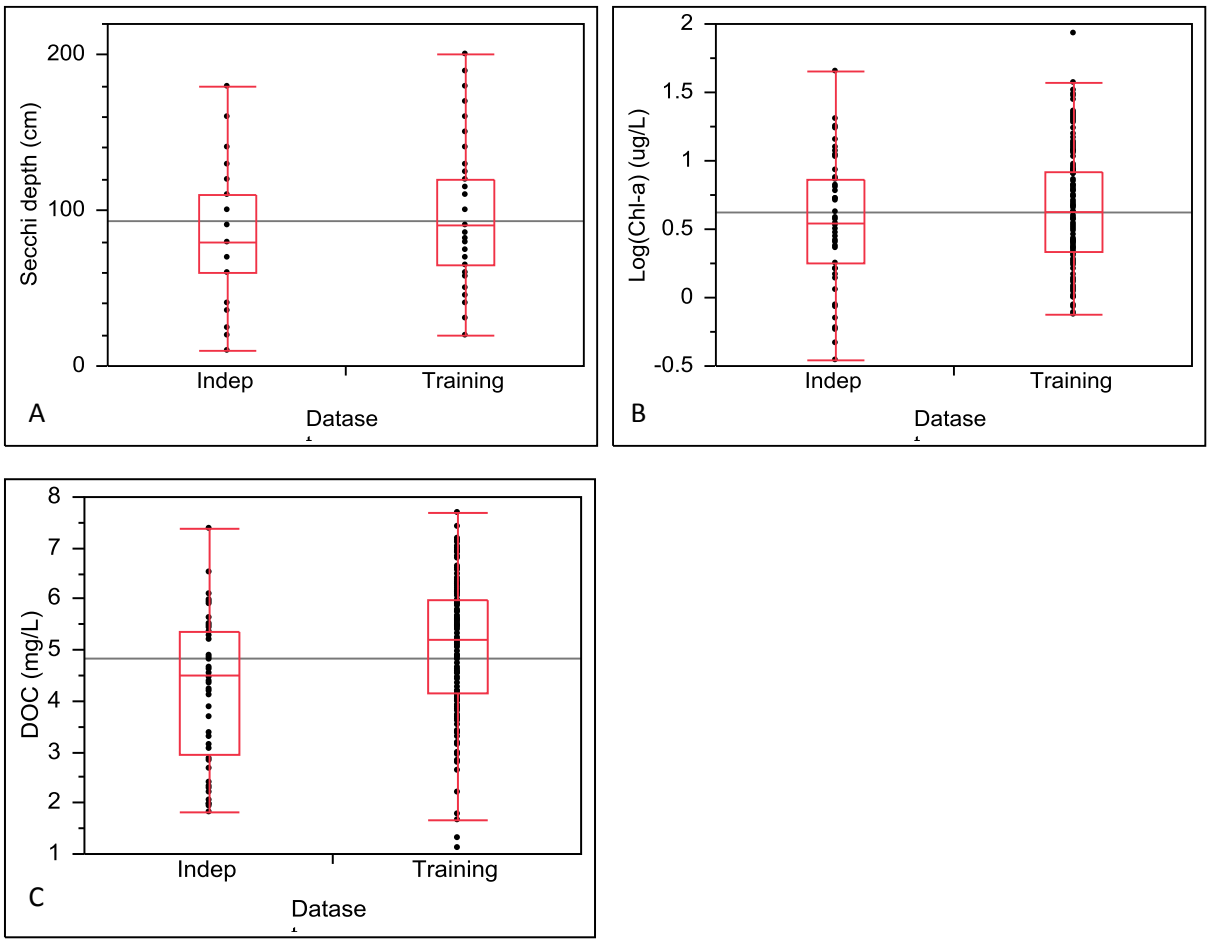

Figure 7: Box and whisker plots comparing the training and validation datasets for Secchi depth (A), Chlorophyll-a (B), and DOC (C).

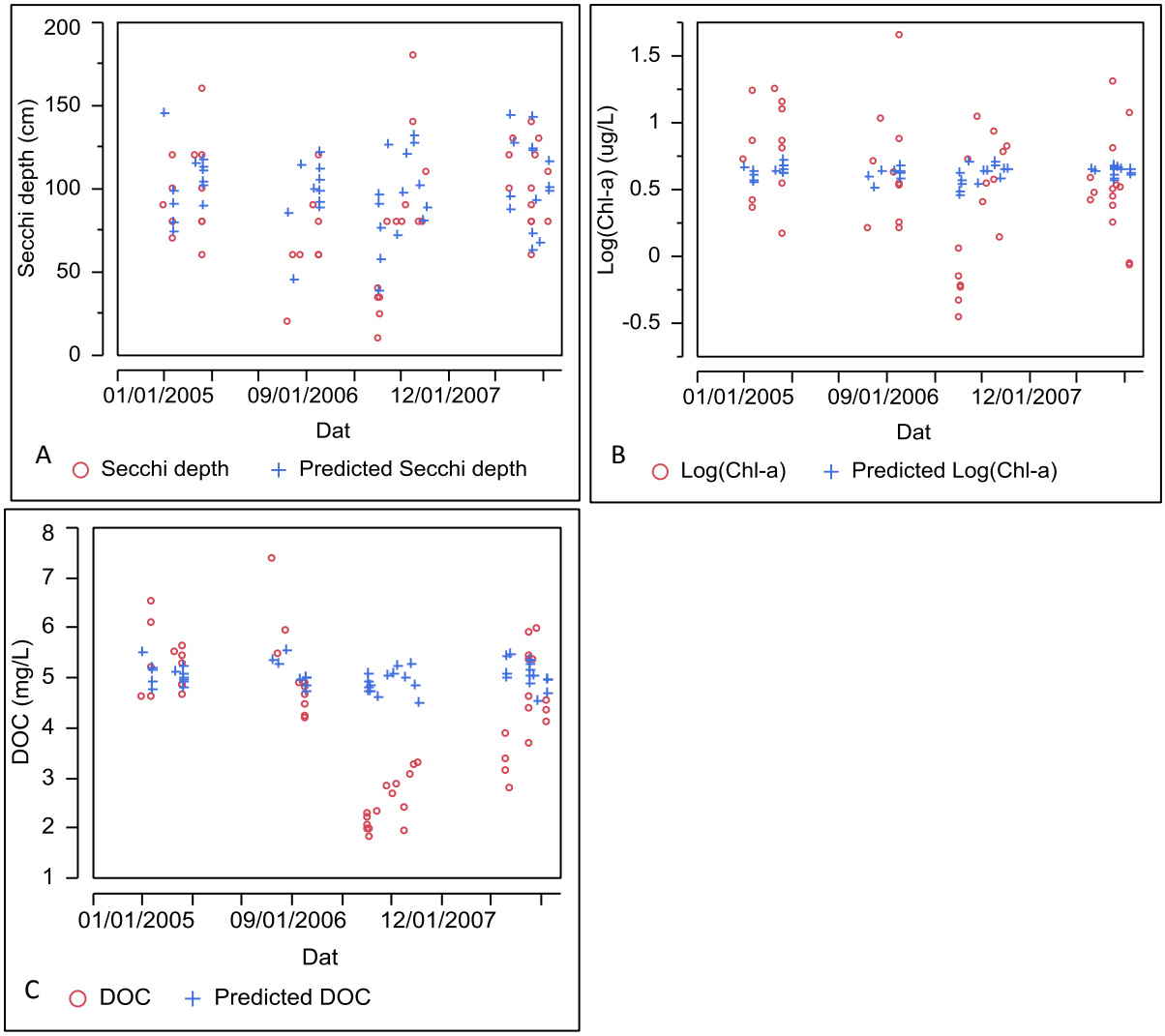

Figure 8: Comparison of predicted and observed values determined using the averaged models for Secchi depth (A), log(Chl-a) (B), and DOC (C) with respect to time.

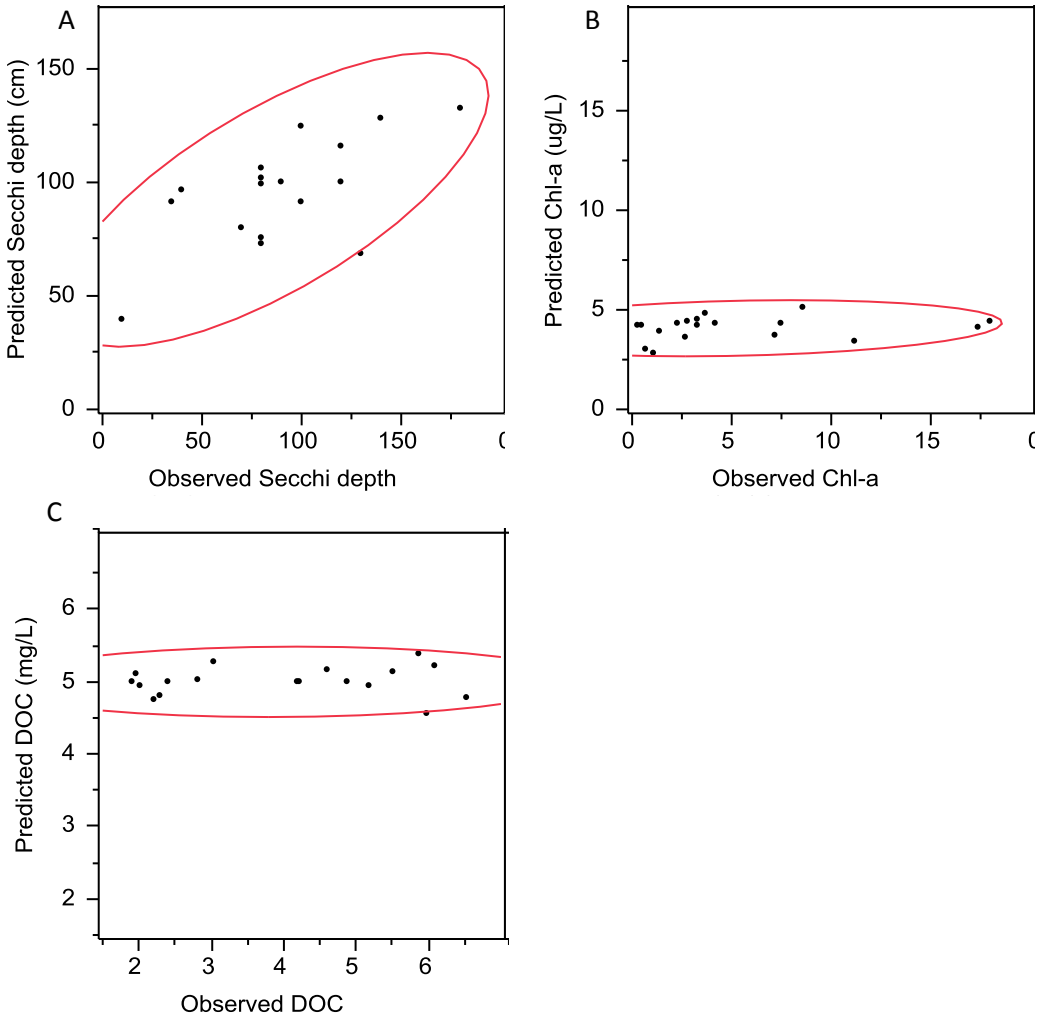

Figure 9: Predicted versus observed values determined using the averaged models for Secchi depth (r=0.72, P= 0.0005) (A); Chl-a (r=0.20, P= 0.43) (B); and DOC (r=0.045, P= 0.85) excluding values where the difference in collection dates was greater than or equal to 2.

WORKS CITED

Abreu, P., M. Bergesch, L. Proença, C. E. Garcia, and C. Odebrecht. 2010. Short- and long-term chlorophyll a variability in the shallow microtidal Patos Lagoon Estuary, Southern Brazil. Estuaries and Coasts **33**:554-569.

Allee, R. J. and J. E. Johnson. 1999. Use of satellite imagery to estimate surface chlorophyll a and Secchi disc depth of Bull Shoals Reservoir, Arkansas, USA. International Journal of Remote Sensing **20**:1057-1072.

Alparslan, E., C. Aydöner, V. Tufekci, and H. Tüfekci. 2007. Water quality assessment at Ömerli Dam using remote sensing techniques. Environmental Monitoring and Assessment **135**:391-398.

Arenz, R. F., W. M. Lewis, and J. F. Saunders. 1996. Determination of chlorophyll and dissolved organic carbon from reflectance data for Colorado reservoirs. International Journal of Remote Sensing **17**:1547-1565.

Baban, S. M. J. 1993. Detecting water quality parameters in the Norfolk Broads, U.K., using Landsat imagery. International Journal of Remote Sensing **14**:1247-1267.

Baban, S. M. J. 1997. Environmental monitoring of estuaries: Estimating and mapping various environmental indicators in Breydon Water Estuary, U.K., using Landsat TM imagery. Estuarine, Coastal and Shelf Science **44**:589-598.

Barbier, E. B., S. D. Hacker, C. Kennedy, E. W. Koch, A. C. Stier, and B. R. Silliman. 2010. The value of estuarine and coastal ecosystem services. Ecological Monographs **81**:169-193.

Borkman, D. G. and T. J. Smayda. 1998. Long-term trends in water clarity revealed by Secchi-disk measurements in lower Narragansett Bay. ICES Journal of Marine Science: Journal du Conseil **55**:668-679.

Brando, V. E. and A. G. Dekker. 2003. Satellite hyperspectral remote sensing for estimating estuarine and coastal water quality. Geoscience and Remote Sensing, IEEE Transactions on **41**:1378-1387.

Brezonik, P., K. D. Menken, and M. Bauer. 2005. Landsat-based remote sensing of lake water quality characteristics, including chlorophyll and colored dissolved organic matter (CDOM). Lake and Reservoir Management **21**:373-382.

Brivio, P. A., C. Giardino, and E. Zilioli. 2001. Determination of chlorophyll concentration changes in Lake Garda using an image-based radiative transfer code for Landsat TM images. International Journal of Remote Sensing **22**:487-502.

Bukata, R. P. 2005. Satellite monitoring of inland and coastal water quality: Retrospection, introspection, future directions. CRC Press, Boca Raton, FL.

Burnham, K. P. and D. R. Anderson. 2002. Model selection and multi-model inference: a practical information-theoretic approach. Springer New York.

Busby, M. W. and K. I. Darmer. 1970. A look at the Hudson River Estuary. Journal of the American Water Resources Association **6**:802-812.

Bustamante, J., F. Pacios, R. Díaz-Delgado, and D. Aragonés. 2009. Predictive models of turbidity and water depth in the Doñana marshes using Landsat TM and ETM+ images. Journal of Environmental Management **90**:2219-2225.

Canty, M. J. and A. A. Nielsen. 2008. Automatic radiometric normalization of multitemporal satellite imagery with the iteratively re-weighted MAD transformation. Remote Sensing of Environment **112**:1025-1036.

Cardille, J. A., J.-B. Leguet, and P. del Giorgio. 2013. Remote sensing of lake CDOM using noncontemporaneous field data. Canadian Journal of Remote Sensing **39**:118-126.

Carpenter, D. J. and S. M. Carpenter. 1983. Modeling inland water quality using Landsat data. Remote Sensing of Environment **13**:345-352.

Carpintero, M., E. Contreras, A. Millares, and M. J. Polo. 2013. Estimation of turbidity along the Guadalquivir estuary using Landsat TM and ETM+ images. Pages 88870B-88870B-88815 *in* Remote Sensing for Agriculture, Ecosystems, and Hydrology XV, Dresden, Germany.

Ceppi, S. B., M. I. Velasco, and C. P. De Pauli. 1999. Differential scanning potentiometry: Surface charge development and apparent dissociation constants of natural humic acids. Talanta **50**:1057-1063.

Chen, L., C.-H. Tan, S.-J. Kao, and T.-S. Wang. 2008. Improvement of remote monitoring on water quality in a subtropical reservoir by incorporating grammatical evolution with parallel genetic algorithms into satellite imagery. Water Research **42**:296-306.

Chernetskiy, M., A. Shevyrnogov, S. Shevnina, G. Vysotskaya, and A. Sidko. 2009. Investigations of the Krasnoyarsk Reservoir waters based on the multispectral satellite data. Advances in Space Research **43**:206-213.

Chica-Olmo, M., F. Rodriguez, F. Abarca, J. P. Rigol-Sanchez, E. deMiguel, J. A. Gomez, and A. Fernandez-Palacios. 2004. Integrated remote sensing and GIS techniques for biogeochemical characterization of the Tinto-Odiel estuary system, SW Spain. Environmental Geology **45**:834-842.

Chipman, J. W., T. M. Lillesand, J. E. Schmaltz, J. E. Leale, and M. J. Nordheim. 2004. Mapping lake water clarity with Landsat images in Wisconsin, USA. Canadian Journal of Remote Sensing **30**:1-7.

D'Sa, E. J. and R. L. Miller. 2003. Bio-optical properties in waters influenced by the Mississippi River during low flow conditions. Remote Sensing of Environment **84**:538-549.

Dekker, A. G., R. J. Vos, and S. W. M. Peters. 2001. Comparison of remote sensing data, model results and in situ data for total suspended matter (TSM) in the southern Frisian lakes. Science of the Total Environment **268**:197-214.

Dekker, A. G., R. J. Vos, and S. W. M. Peters. 2002. Analytical algorithms for lake water TSM estimation for retrospective analyses of TM and SPOT sensor data. International Journal of Remote Sensing **23**:15-35.

Dor, I. and N. Ben-Yosef. 1996. Monitoring effluent quality in hypertrophic wastewater reservoirs using remote sensing. Water Science and Technology **33**:23-29.

Doxaran, D., P. Castaing, and S. J. Lavender. 2006. Monitoring the maximum turbidity zone and detecting fine-scale turbidity features in the Gironde estuary using high spatial resolution satellite sensor (SPOT HRV, Landsat ETM+) data. International Journal of Remote Sensing **27**:2303-2321.

Doxaran, D., R. C. N. Cherukuru, and S. J. Lavender. 2005. Use of reflectance band ratios to estimate suspended and dissolved matter concentrations in estuarine waters. International Journal of Remote Sensing **26**:1763-1769.

Doxaran, D., J.-M. Froidefond, and P. Castaing. 2003. Remote-sensing reflectance of turbid sediment-dominated waters: Reduction of sediment type variations and changing illumination conditions effects by use of reflectance ratios. Appl. Opt. **42**:2623-2634.

Doxaran, D., J.-M. Froidefond, S. Lavender, and P. Castaing. 2002. Spectral signature of highly turbid waters: Application with SPOT data to quantify suspended particulate matter concentrations. Remote Sensing of Environment **81**:149-161.

Ekstrand, S. 1992. Landsat TM based quantification of chlorophyll-a during algae blooms in coastal waters. International Journal of Remote Sensing **13**:1913-1926.

Findlay, S., D. Strayer, C. Goumbala, and K. Gould. 1993. Metabolism of streamwater dissolved organic carbon in the shallow hyporheic zone. Limnology and Oceanography **38**:1493-1499.

Findlay, S. E. G. 2005. Increased carbon transport in the Hudson River: Unexpected consequence of nitrogen deposition? Frontiers in Ecology and the Environment **3**:133-137.

Findlay, S. E. G. and R. L. Sinsabaugh. 2003. Aquatic ecosystems: Interactivity of dissolved organic matter. Elsevier, USA.

Fleming-Lehtinen, V. and M. Laamanen. 2012. Long-term changes in Secchi depth and the role of phytoplankton in explaining light attenuation in the Baltic Sea. Estuarine, Coastal and Shelf Science **102–103**:1-10.

Freeman, W. O. 1991. National Water-Quality Assessment Program-- The Hudson River Basin. 91-166, U.S.Geological Survey.

Frenette, J.-J., M. Arts, and J. Morin. 2003. Spectral gradients of downwelling light in a fluvial lake (Lake Saint-Pierre, St-Lawrence River). Aquatic Ecology **37**:77-85.

Gallegos, C. L., P. J. Werdell, and C. R. McClain. 2011. Long-term changes in light scattering in Chesapeake Bay inferred from Secchi depth, light attenuation, and remote sensing measurements. Journal of Geophysical Research: Oceans **116**:C00H08.

García-Gil, J. C., S. B. Ceppi, M. I. Velasco, A. Polo, and N. Senesi. 2004. Long-term effects of amendment with municipal solid waste compost on the elemental and acidic functional group composition and pH-buffer capacity of soil humic acids. Geoderma **121**:135-142.

Giardino, C., V. E. Brando, A. G. Dekker, N. Strömbeck, and G. Candiani. 2007. Assessment of water quality in Lake Garda (Italy) using Hyperion. Remote Sensing of Environment **109**:183-195.

Giardino, C., M. Pepe, P. A. Brivio, P. Ghezzi, and E. Zilioli. 2001. Detecting chlorophyll, Secchi disk depth and surface temperature in a sub-alpine lake using Landsat imagery. Science of the Total Environment **268**:19-29.

Gibson, L. A., B. A. Wilson, D. M. Cahill, and J. Hill. 2004. Spatial prediction of rufous bristlebird habitat in a coastal heathland: a GIS-based approach. Journal of Applied Ecology **41**:213-223.

Gitelson, A., G. Garbuzov, F. Szilagyi, K. H. Mittenzwey, A. Karnieli, and A. Kaiser. 1993. Quantitative remote-sensing methods for real-time monitoring of inland water quality. International Journal of Remote Sensing **14**:1269-1295.

Gons, H. J. 1999. Optical teledetection of chlorophyll-a in turbid inland waters. Environmental Science & Technology **33**:1127-1132.

Hadjimitsis, D. and C. Clayton. 2009. Assessment of temporal variations of water quality in inland water bodies using atmospheric corrected satellite remotely sensed image data. Environmental Monitoring and Assessment **159**:281-292.

Hadjimitsis, D. G., C. R. I. Clayton, and V. S. Hope. 2004. An assessment of the effectiveness of atmospheric correction algorithms through the remote sensing of some reservoirs. International Journal of Remote Sensing **25**:3651-3674.

Han, L. and K. J. Jordan. 2005. Estimating and mapping chlorophyll-a concentration in Pensacola Bay, Florida using Landsat ETM+ data. International Journal of Remote Sensing **26**:5245-5254.

Harrington Jr, J. A., F. R. Schiebe, and J. F. Nix. 1992. Remote sensing of Lake Chicot, Arkansas: Monitoring suspended sediments, turbidity, and Secchi depth with Landsat MSS data. Remote Sensing of Environment **39**:15-27.

Hayakawa, K. and Y. Sugiyama. 2008. Spatial and seasonal variations in attenuation of solar ultraviolet radiation in Lake Biwa, Japan. Journal of Photochemistry and Photobiology B: Biology **90**:121-133.

Hays, G. C., A. J. Richardson, and C. Robinson. 2005. Climate change and marine plankton. Trends in Ecology & Evolution **20**:337-344.

Hellweger, F. L., P. Schlosser, U. Lall, and J. K. Weissel. 2004. Use of satellite imagery for water quality studies in New York Harbor. Estuarine Coastal and Shelf Science **61**:437-448.

Hirtle, H. and A. Rencz. 2003. The relation between spectral reflectance and dissolved organic carbon in lake water: Kejimkujik National Park, Nova Scotia, Canada. International Journal of Remote Sensing **24**:953-967.

Kabbara, N., J. Benkhelil, M. Awad, and V. Barale. 2008. Monitoring water quality in the coastal area of Tripoli (Lebanon) using high-resolution satellite data. ISPRS Journal of Photogrammetry and Remote Sensing **63**:488-495.

Kallio, K., J. Attila, P. Harma, S. Koponen, J. Pulliainen, U. M. Hyytiainen, and T. Pyhalahti. 2008. Landsat ETM+ images in the estimation of seasonal lake water quality in boreal river basins. Environmental Management **42**:511-522.

Khorram, S., H. Cheshire, A. L. Geraci, and G. L. Rosa. 1991. Water quality mapping of Augusta Bay, Italy from Landsat-TM data. International Journal of Remote Sensing **12**:803-808.

Kloiber, S. M., P. L. Brezonik, and M. E. Bauer. 2002a. Application of Landsat imagery to regional-scale assessments of lake clarity. Water Research **36**:4330-4340.

Kloiber, S. N., P. L. Brezonik, L. G. Olmanson, and M. E. Bauer. 2002b. A procedure for regional lake water clarity assessment using Landsat multispectral data. Remote Sensing of Environment **82**:38-47.

Kondratyev, K. Y., D. V. Pozdnyakov, and L. H. Pettersson. 1998. Water quality remote sensing in the visible spectrum. International Journal of Remote Sensing **19**:957-979.

Kutser, T., D. Pierson, L. Tranvik, A. Reinart, S. Sobek, and K. Kallio. 2005a. Using satellite remote sensing to estimate the colored dissolved organic matter absorption coefficient in lakes. Ecosystems **8**:709-720.

Kutser, T., D. C. Pierson, K. Y. Kallio, A. Reinart, and S. Sobek. 2005b. Mapping lake CDOM by satellite remote sensing. Remote Sensing of Environment **94**:535-540.

Kutser, T., L. Tranvik, and D. C. Pierson. 2009. Variations in colored dissolved organic matter between boreal lakes studied by satellite remote sensing. Journal of Applied Remote Sensing **3**:10.

Larkin, J. 2010. Sample Stations: Hudson River, New York.

Lathrop, R. G. 1992. Landsat Thematic Mapper monitoring of turbid inland water-quality. Photogrammetric Engineering and Remote Sensing **58**:465-470.

Lathrop, R. G. and T. M. Lillesand. 1986. Use of thematic mapper data to assess water-quality in Green Bay and central Lake Michigan. Photogrammetric Engineering and Remote Sensing **52**:671-680.

Lavery, P., C. Pattiaratchi, A. Wyllie, and P. Hick. 1993. Water quality monitoring in estuarine waters using the landsat thematic mapper. Remote Sensing of Environment **46**:268-280.

Lennon, J. T. 2004. Experimental evidence that terrestrial carbon subsidies increase CO2 flux from lake ecosystems. Oecologia **138**:584-591.

Lillesand, T. M., W. L. Johnson, R. L. Deuell, O. M. Lindstrom, and D. E. Meisner. 1983. Use of Landsat data to predict the trophic state of Minnesota lakes. Photogrammetric Engineering and Remote Sensing **49**:219-229.

Lotze, H. K., H. S. Lenihan, B. J. Bourque, R. H. Bradbury, R. G. Cooke, M. C. Kay, S. M. Kidwell, M. X. Kirby, C. H. Peterson, and J. B. C. Jackson. 2006. Depletion, degradation, and recovery potential of estuaries and coastal seas. Science **312**:1806-1809.

Ma, R., J. Tang, and J. Dai. 2006. Bio-optical model with optimal parameter suitable for Taihu Lake in water colour remote sensing. International Journal of Remote Sensing **27**:4305-4328.

Mantas, V. M., A. J. S. C. Pereira, J. Neto, J. Patricio, and J. C. Marques. 2013. Monitoring estuarine water quality using satellite imagery. The Mondego river estuary (Portugal) as a case study. Ocean & Coastal Management **72**:13-21.

Matthews, M. W. 2011. A current review of empirical procedures of remote sensing in inland and near-coastal transitional waters. International Journal of Remote Sensing **32**:6855-6899.

McCrone, A. W. 1966. The Hudson River Estuary: Hydrology, sediments, and pollution. Geographical Review **56**:175-189.

McQuatters-Gollop, A., D. E. Raitsos, M. Edwards, Y. Pradhan, L. D. Mee, S. J. Lavender, and M. J. Attrill. 2007. A long-term chlorophyll data set reveals regime shift in North Sea phytoplankton biomass unconnected to nutrient trends. Limnology and Oceanography **52**:635-648.

Monbet, Y. 1992. Control of phytoplankton biomass in estuaries: A comparative analysis of microtidal and macrotidal estuaries. Estuaries **15**:563-571.

Nielsen, A. A. 2007. The regularized iteratively reweighted MAD method for change detection in multi- and hyperspectral data. IEEE Transactions on Image Processing **16**:463-478.

Olmanson, L. G., M. E. Bauer, and P. L. Brezonik. 2008. A 20-year Landsat water clarity census of Minnesota's 10,000 lakes. Remote Sensing of Environment **112**:4086-4097.

Paerl, H. W., L. M. Valdes, J. L. Pinckney, M. F. Piehler, J. Dyble, and P. H. Moisander. 2003. Phytoplankton photopigments as indicators of estuarine and coastal eutrophication. BioScience **53**:953-964.

Pattiaratchi, C., P. Lavery, A. Wyllie, and P. Hick. 1994. Estimates of water quality in coastal waters using multi-date Landsat Thematic Mapper data. International Journal of Remote Sensing **15**:1571-1584.

Richter, R. 1996. A spatially adaptive fast atmospheric correction algorithm. International Journal of Remote Sensing **17**:1201-1214.

Richter, R. 1997. Correction of atmospheric and topographic effects for high spatial resolution satellite imagery. International Journal of Remote Sensing **18**:1099-1111.

Richter, R. 2010. ATCOR for ERDAS Imagine 2010. GEOSYSTEMS GmbH.

Roulet, N. and T. R. Moore. 2006. Environmental chemistry: Browning the waters. Nature **444**:283-284.

Ruddick, K. G., H. J. Gons, M. Rijkeboer, and G. Tilstone. 2001. Optical remote sensing of Chlorophyll a in case 2 waters by use of an adaptive two-band algorithm with optimal error properties. Applied Optics **40**:3575-3585.

Sathyendranath, S., L. Prieur, and A. Morel. 1989. A three-component model of ocean colour and its application to remote sensing of phytoplankton pigments in coastal waters. International Journal of Remote Sensing **10**:1373-1394.

Sawaya, K. E., L. G. Olmanson, N. J. Heinert, P. L. Brezonik, and M. E. Bauer. 2003. Extending satellite remote sensing to local scales: land and water resource monitoring using high-resolution imagery. Remote Sensing of Environment **88**:144-156.

Stevens, J. P. 1984. Outliers and influential data points in regression analysis. Pages 334-344. American Psychological Association, US.

Strayer, D. L. and L. C. Smith. 2001. The zoobenthos of the freshwater tidal Hudson River and its response to the zebra mussel (*Dreissena polymorpha*) invasion. Arch. Hydrobiol. Suppl. (Monographic Studies) **139**.

Studies, C. I. o. E. 2009. HRCardinal.*in* C. I. o. E. Studies, editor., Millbrook, NY.

Sváb, E., A. N. Tyler, T. Preston, M. Présing, and K. V. Balogh. 2005. Characterizing the spectral reflectance of algae in lake waters with high suspended sediment concentrations. International Journal of Remote Sensing **26**:919-928.

Vertucci, F. A. and G. E. Likens. 1989. Spectral reflectance and water quality of Adirondak Mountain region lakes. Limnology and Oceanography **34**:1656-1672.

Vincent, R. K., X. Qin, R. M. L. McKay, J. Miner, K. Czajkowski, J. Savino, and T. Bridgeman. 2004. Phycocyanin detection from Landsat TM data for mapping cyanobacterial blooms in Lake Erie. Remote Sensing of Environment **89**:381-392.

Vos, R. J., J. H. M. Hakvoort, R. W. J. Jordans, and B. W. Ibelings. 2003. Multiplatform optical monitoring of eutrophication in temporally and spatially variable lakes. Science of the Total Environment **312**:221-243.

Wang, F., L. Han, H. T. Kung, and R. B. Van Arsdale. 2006. Applications of Landsat-5 TM imagery in assessing and mapping water quality in Reelfoot Lake, Tennessee. International Journal of Remote Sensing **27**:5269-5283.

Wang, Y. P., H. Xia, J. M. Fu, and G. Y. Sheng. 2004. Water quality change in reservoirs of Shenzhen, China: detection using LANDSAT/TM data. Science of the Total Environment **328**:195-206.

Wurtsbaugh, W. A. and T. S. Berry. 1990. Cascading effects of decreased salinity on the plankton chemistry, and physics of the Great Salt Lake (Utah). Canadian Journal of Fisheries and Aquatic Sciences **47**:100-109.

Yamashita, Y. and R. Jaffé. 2008. Characterizing the interactions between trace metals and dissolved organic matter using excitation−emission matrix and parallel factor analysis. Environmental Science & Technology **42**:7374-7379.

Yamashita, Y., L. Scinto, N. Maie, and R. Jaffé. 2010. Dissolved organic matter characteristics across a subtropical wetland's landscape: Application of optical properties in the assessment of environmental dynamics. Ecosystems **13**:1006-1019.

Appendix A

Table A1. Best subset of models for Secchi depth

Model	K	AIC	AICc	Delta AICC (Δ_i)	Relative Likelihood	Akaike (w_i)	Model Variables
1	5	1114.016	1114.4	0	1	0.027916	B1 B3 B1_B3 B2_B3 B2_B4
2	5	1114.178	1114.562	0.1619	0.92224	0.025745	B1 B3 B1_B3 B1_B4 B2_B3
3	5	1114.188	1114.573	0.1722	0.917502	0.025613	B1 B2 B1_B3 B2_B3 B4_B2
4	5	1114.207	1114.592	0.1915	0.908691	0.025367	B2 B1_B2 B1_B3 B2_B3 B4_B2
5	6	1114.117	1114.658	0.25802	0.878965	0.024537	B3 B1_B2 B1_B3 B2_B3 B2_B4 B4_B2
6	6	1114.226	1114.768	0.36732	0.832219	0.023232	B2 B1_B2 B1_B3 B2_B3 B2_B4 B4_B2
7	4	1114.552	1114.807	0.406562	0.816049	0.022781	B1 B3 B1_B3 B2_B3
8	6	1114.313	1114.855	0.45422	0.796833	0.022245	B1 B2 B1_B3 B2_B3 B2_B4 B4_B2
9	5	1114.5	1114.885	0.4845	0.78486	0.02191	B3 B1_B2 B1_B3 B2_B3 B4_B2
10	6	1114.429	1114.971	0.57032	0.751894	0.02099	B3 B1_B2 B1_B3 B1_B4 B2_B3 B4_B2
11	6	1114.56	1115.102	0.70182	0.704047	0.019654	B1 B3 B1_B3 B2_B3 B2_B4 B3_B4
12	6	1114.58	1115.122	0.72142	0.697181	0.019463	B1 B2 B1_B3 B1_B4 B2_B3 B4_B2
13	6	1114.611	1115.153	0.75272	0.686355	0.01916	B2 B1_B2 B1_B3 B1_B4 B2_B3 B4_B2

Table A2

Model	K	AIC	AICc	Delta AICC (Δ_i)	Relative Likelihood	Akaike (w_i)	Model Variables
14	5	1114.897	1115.281	0.881	0.643714	0.01797	B1 B3 B1_B3 B2_B3 B3_B4
15	6	1114.746	1115.288	0.88732	0.641684	0.017913	B1 B3 B1_B3 B1_B4 B2_B3 B3_B4
16	5	1114.926	1115.311	0.9106	0.634258	0.017706	B3 B1_B2 B1_B3 B2_B3 B2_B4
17	4	1115.059	1115.313	0.912962	0.633509	0.017685	B3 B1_B2 B1_B3 B2_B3
18	6	1114.912	1115.454	1.05392	0.590397	0.016482	B2 B1_B2 B1_B3 B2_B3 B3_B4 B4_B2
19	6	1114.916	1115.457	1.05702	0.589483	0.016456	B3 B1_B2 B1_B3 B2_B3 B3_B4 B4_B2
20	6	1115.002	1115.543	1.14302	0.564672	0.015763	B1 B2 B1_B3 B2_B3 B3_B4 B4_B2
21	5	1115.202	1115.587	1.1864	0.552556	0.015425	B3 B1_B3 B2_B3 B2_B4 B3_B1
22	7	1114.879	1115.606	1.205457	0.547316	0.015279	B3 B1_B2 B1_B3 B2_B3 B2_B4 B3_B4 B4_B2
23	6	1115.079	1115.621	1.22032	0.543264	0.015166	B1 B3 B4 B1_B3 B2_B3 B2_B4
24	5	1115.27	1115.655	1.2541	0.534165	0.014912	B3 B1_B2 B1_B3 B1_B4 B2_B3
25	6	1115.176	1115.718	1.31792	0.517389	0.014444	B1 B3 B4 B1_B3 B1_B4 B2_B3
26	6	1115.228	1115.77	1.36972	0.504161	0.014074	B1 B3 B1_B3 B2_B3 B2_B4 B4_B3
27	7	1115.091	1115.818	1.417657	0.49222	0.013741	B1 B2 B1_B3 B2_B3 B2_B4 B3_B4 B4_B2

Table A3

Model	K	AIC	AICc	Delta AICC (Δ_i)	Relative Likelihood	Akaike (w_i)	Model Variables
29	6	1115.292	1115.834	1.43332	0.488381	0.013634	B3 B1_B2 B1_B3 B2_B3 B2_B4 B3_B4
28	7	1115.109	1115.837	1.436157	0.487688	0.013614	B2 B1_B2 B1_B3 B2_B3 B2_B4 B3_B4 B4_B2
30	6	1115.331	1115.873	1.47232	0.47895	0.01337	B1 B2 B4 B1_B3 B2_B3 B4_B2
31	6	1115.333	1115.875	1.47492	0.478327	0.013353	B1 B3 B1_B3 B1_B4 B2_B3 B4_B3
32	5	1115.491	1115.876	1.4755	0.478189	0.013349	B3 B1_B3 B1_B4 B2_B3 B3_B1
33	7	1115.173	1115.9	1.499457	0.472495	0.01319	B3 B1_B2 B1_B3 B2_B3 B2_B4 B4_B2 B4_B3
34	7	1115.265	1115.992	1.591557	0.45123	0.012597	B3 B4 B1_B2 B1_B3 B2_B3 B2_B4 B4_B2
35	6	1115.494	1116.036	1.63532	0.441463	0.012324	B2 B1_B2 B1_B3 B2_B3 B4_B2 B4_B3
36	6	1115.525	1116.067	1.66642	0.434652	0.012134	B1 B3 B1_B2 B1_B3 B2_B3 B2_B4
37	6	1115.525	1116.067	1.66692	0.434543	0.012131	B2 B4 B1_B2 B1_B3 B2_B3 B4_B2
38	6	1115.528	1116.07	1.66992	0.433892	0.012113	B3 B1_B2 B1_B3 B2_B3 B4_B2 B4_B3
39	6	1115.53	1116.072	1.67162	0.433523	0.012102	B1 B2 B3 B1_B3 B2_B3 B2_B4
40	5	1115.696	1116.08	1.68	0.431711	0.012052	B1 B2 B3 B1_B3 B2_B3
41	5	1115.708	1116.093	1.6921	0.429107	0.011979	B1 B3 B4 B1_B3 B2_B3

Table A4

Model	K	AIC	AICc	Delta AICC (Δ_i)	Relative Likelihood	Akaike (w_i)	Model Variables
42	6	1115.564	1116.106	1.70592	0.426152	0.011897	B1 B2 B3 B1_B3 B2_B3 B4_B2
43	6	1115.584	1116.126	1.72512	0.42208	0.011783	B1 B2 B1_B2 B1_B3 B2_B3 B4_B2
44	5	1115.76	1116.145	1.7444	0.418031	0.01167	B3 B1_B2 B1_B3 B2_B3 B3_B4
46	6	1115.626	1116.168	1.76732	0.413268	0.011537	B3 B1_B3 B2_B3 B2_B4 B3_B4 B3_B1
45	7	1115.446	1116.173	1.772857	0.412125	0.011505	B1 B2 B4 B1_B3 B2_B3 B2_B4 B4_B2
49	5	1115.79	1116.175	1.7742	0.411848	0.011497	B1 B3 B1_B2 B1_B3 B2_B3
47	7	1115.45	1116.178	1.777257	0.411219	0.01148	B3 B1_B2 B1_B3 B1_B4 B2_B3 B4_B2 B4_B3
48	6	1115.638	1116.18	1.77962	0.410734	0.011466	B1 B2 B1_B3 B2_B3 B4_B2 B4_B3
51	5	1115.803	1116.188	1.7873	0.40916	0.011422	B1 B3 B1_B3 B2_B3 B4_B3
50	7	1115.475	1116.202	1.801657	0.406233	0.01134	B1 B2 B3 B1_B3 B2_B3 B2_B4 B4_B2
52	6	1115.683	1116.225	1.82442	0.401636	0.011212	B3 B4 B1_B2 B1_B3 B2_B3 B4_B2
53	7	1115.519	1116.247	1.846257	0.397274	0.01109	B2 B4 B1_B2 B1_B3 B2_B3 B2_B4 B4_B2
54	7	1115.532	1116.259	1.858457	0.394858	0.011023	B2 B1_B2 B1_B3 B2_B3 B2_B4 B4_B2 B4_B3
57	6	1115.721	1116.262	1.86202	0.394155	0.011003	B2 B3 B1_B2 B1_B3 B2_B3 B4_B2

Table A5

Model	K	AIC	AICc	Delta AICC (Δ_i)	Relative Likelihood	Akaike (w_i)	Model Variables
58	6	1115.721	1116.263	1.86242	0.394077	0.011001	B1 B2 B1_B3 B2_B3 B3_B2 B4_B2
63	4	1116.01	1116.265	1.864162	0.393734	0.010992	B3 B1_B3 B2_B3 B3_B1
64	4	1116.01	1116.265	1.864162	0.393734	0.010992	B3 B1_B3 B2_B3 B2_B4
55	7	1115.539	1116.266	1.865557	0.393459	0.010984	B2 B3 B1_B2 B1_B3 B2_B3 B2_B4 B4_B2
56	7	1115.542	1116.269	1.868957	0.392791	0.010965	B3 B4 B1_B2 B1_B3 B1_B4 B2_B3 B4_B2
59	6	1115.731	1116.272	1.87202	0.39219	0.010948	B1 B2 B3 B1_B3 B1_B4 B2_B3
61	6	1115.742	1116.284	1.88352	0.389941	0.010886	B1 B3 B1_B3 B2_B3 B2_B4 B3_B1
62	6	1115.745	1116.287	1.88662	0.389337	0.010869	B1 B3 B1_B3 B2_B3 B2_B4 B3_B2
60	7	1115.56	1116.287	1.886957	0.389271	0.010867	B2 B1_B2 B1_B3 B1_B4 B2_B3 B2_B4 B4_B2
65	6	1115.753	1116.295	1.89482	0.387744	0.010824	B1 B3 B1_B2 B1_B3 B1_B4 B2_B3
66	6	1115.824	1116.366	1.96542	0.374295	0.010449	B1 B3 B1_B3 B2_B3 B2_B4 B4_B2
67	6	1115.824	1116.366	1.96592	0.374202	0.010446	B1 B3 B1_B3 B2_B3 B2_B4 B2_B1
68	7	1115.671	1116.398	1.997957	0.368255	0.01028	B1 B2 B4 B1_B3 B1_B4 B2_B3 B4_B2

Appendix B

Table B1. Best subset of models for Log(Chl-a)

Model	K	AIC	AICc	Delta AIC_C (Δ_i)	Relative Likelihood	Akaike (w_i)	Model Variables
1	1	702.1344	702.1602	0	1	0.180478	B2
2	1	703.3293	703.3551	1.1949	0.550213	0.099301	B3
3	2	703.7232	703.8011	1.640916	0.44023	0.079452	B2 B2_B3
4	2	703.7594	703.8373	1.677116	0.432334	0.078027	B1 B2
5	2	703.8846	703.9625	1.802316	0.406099	0.073292	B2 B2_B4
6	2	703.8882	703.9661	1.805916	0.405369	0.07316	B2 B1_B4
7	2	703.9093	703.9872	1.827016	0.401115	0.072392	B2 B3_B4
8	2	703.9115	703.9894	1.829216	0.400674	0.072313	B2 B3
9	2	703.9986	704.0765	1.916316	0.383599	0.069231	B2 B1_B3
10	2	704.0396	704.1175	1.957316	0.375815	0.067826	B2 B3_B1
11	2	704.0398	704.1177	1.957516	0.375778	0.067819	B2 B2_B1
12	2	704.0728	704.1507	1.990516	0.369628	0.06671	B2 B4

Appendix C

Table C1. Best subset of models for DOC

Model	K	AIC	AICc	Delta AIC_C (Δ_i)	Relative Likelihood	Akaike (w_i)	Model Variables
1	4	88.4978	88.75258	0	1	0.008595	B1 B2 B4 B2_B4
3	4	88.6082	88.86298	0.1104	0.946296	0.008133	B4 B1_B2 B1_B3 B2_B4
4	4	88.6564	88.91118	0.1586	0.923763	0.00794	B1 B2 B4 B1_B4
2	2	88.8514	88.92687	0.174295	0.916542	0.007878	B4 B3_B1
6	5	88.5727	88.95732	0.204738	0.902696	0.007759	B1 B2 B4 B1_B3 B2_B4
5	3	88.8866	89.0385	0.285922	0.866788	0.00745	B4 B2_B4 B3_B1
7	3	88.9103	89.0622	0.309622	0.856577	0.007362	B2 B4 B3_B1
8	4	88.842	89.09678	0.3442	0.841895	0.007236	B4 B1_B2 B1_B3 B1_B4
9	4	88.912	89.16678	0.4142	0.812938	0.006987	B2 B4 B2_B4 B3_B1
15	5	88.8179	89.20252	0.449938	0.798541	0.006863	B1 B2 B4 B1_B3 B1_B4
12	3	89.101	89.2529	0.500322	0.778676	0.006693	B4 B1_B4 B3_B1
13	3	89.1016	89.2535	0.500922	0.778442	0.006691	B1 B2 B4
10	2	89.1859	89.26137	0.508795	0.775384	0.006664	B3 B4
11	2	89.1881	89.26357	0.510995	0.774531	0.006657	B4 B1_B3
16	4	89.0191	89.27388	0.5213	0.770551	0.006623	B4 B2_B4 B3_B4 B3_B1
14	3	89.1361	89.288	0.535422	0.765129	0.006576	B4 B1_B3 B2_B4
18	4	89.0349	89.28968	0.5371	0.764487	0.006571	B2 B4 B1_B4 B3_B1
17	3	89.17	89.3219	0.569322	0.752269	0.006466	B4 B1_B2 B1_B3
20	5	88.9453	89.32992	0.577338	0.74926	0.00644	B1 B2 B4 B2_B4 B3_B4

Table C2

Model	K	AIC	AICc	Delta AIC_C (Δ_i)	Relative Likelihood	Akaike (w_i)	Model Variables
21	5	88.9778	89.36242	0.609838	0.737183	0.006336	B4 B1_B2 B1_B3 B2_B4 B3_B4
19	2	89.3747	89.45017	0.697595	0.705536	0.006064	B2 B4
25	4	89.1991	89.45388	0.7013	0.70423	0.006053	B1 B2 B4 B1_B3
22	3	89.3188	89.4707	0.718122	0.698332	0.006002	B4 B1_B2 B2_B4
23	3	89.3274	89.4793	0.726722	0.695335	0.005976	B2 B4 B2_B4
24	3	89.3305	89.4824	0.729822	0.694259	0.005967	B4 B1_B3 B3_B1
27	4	89.2367	89.49148	0.7389	0.691114	0.00594	B3 B4 B1_B2 B2_B4
26	3	89.378	89.5299	0.777322	0.677964	0.005827	B3 B4 B2_B4
36	5	89.156	89.54062	0.788038	0.674341	0.005796	B1 B2 B4 B1_B4 B3_B4
28	3	89.403	89.5549	0.802322	0.669542	0.005755	B2 B4 B1_B3
29	3	89.4044	89.5563	0.803722	0.669074	0.005751	B4 B1_B3 B1_B4
30	3	89.4193	89.5712	0.818622	0.664108	0.005708	B2 B4 B1_B4
31	3	89.4262	89.5781	0.825522	0.661821	0.005688	B3 B4 B3_B1
34	4	89.3271	89.58188	0.8293	0.660571	0.005678	B4 B1_B3 B2_B4 B3_B1
35	4	89.3279	89.58268	0.8301	0.660307	0.005675	B2 B4 B1_B3 B2_B4
37	4	89.3388	89.59358	0.841	0.656718	0.005644	B3 B4 B1_B2 B1_B4
41	5	89.2163	89.60092	0.848338	0.654313	0.005624	B1 B2 B4 B2_B3 B2_B4
32	3	89.469	89.6209	0.868322	0.647808	0.005568	B4 B3_B1 B3_B2
33	3	89.4701	89.622	0.869422	0.647452	0.005565	B4 B1_B2 B1_B4
38	3	89.5026	89.6545	0.901922	0.637016	0.005475	B3 B4 B1_B2
43	4	89.4013	89.65608	0.9035	0.636513	0.005471	B4 B2_B4 B3_B1 B3_B2

Table C3

Model	K	AIC	AICc	Delta AIC_C (Δ_i)	Relative Likelihood	Akaike (w_i)	Model Variables
39	3	89.5158	89.6677	0.915122	0.632825	0.005439	B3 B4 B1_B3
40	3	89.5184	89.6703	0.917722	0.632003	0.005432	B3 B4 B1_B4
44	4	89.4186	89.67338	0.9208	0.631031	0.005424	B1 B2 B4 B3_B4
52	6	89.1546	89.69654	0.943958	0.623766	0.005361	B1 B2 B4 B1_B3 B2_B4 B3_B4
45	4	89.4554	89.71018	0.9576	0.619526	0.005325	B4 B1_B2 B2_B4 B3_B4
47	4	89.4748	89.72958	0.977	0.613546	0.005273	B4 B1_B3 B2_B4 B3_B4
42	2	89.6565	89.73197	0.979395	0.612812	0.005267	B3_B1 B4_B3
53	5	89.3618	89.74642	0.993838	0.608402	0.005229	B2 B4 B2_B4 B3_B4 B3_B1
50	4	89.4991	89.75388	1.0013	0.606137	0.00521	B2 B4 B1_B3 B1_B4
46	3	89.6165	89.7684	1.015822	0.601751	0.005172	B3 B4 B2_B1
51	4	89.5177	89.77248	1.0199	0.600526	0.005162	B4 B1_B2 B2_B3 B2_B4
48	3	89.6294	89.7813	1.028722	0.597883	0.005139	B1 B3 B4
49	3	89.6321	89.784	1.031422	0.597076	0.005132	B2_B4 B3_B1 B4_B3
54	4	89.5397	89.79448	1.0419	0.593956	0.005105	B4 B1_B2 B1_B3 B3_B4
55	4	89.5516	89.80638	1.0538	0.590432	0.005075	B2 B4 B1_B2 B2_B4
63	5	89.4299	89.81452	1.061938	0.588035	0.005054	B1 B2 B4 B1_B4 B2_B3
56	4	89.5697	89.82448	1.0719	0.585113	0.005029	B4 B1_B2 B1_B4 B3_B4

Table C4

Model	K	AIC	AICc	Delta AIC_C (Δ_i)	Relative Likelihood	Akaike (w_i)	Model Variables
66	5	89.4465	89.83112	1.078538	0.583174	0.005012	B3 B4 B1_B2 B1_B3 B2_B4
59	4	89.5781	89.83288	1.0803	0.582661	0.005008	B2 B4 B2_B4 B2_B1
61	4	89.5937	89.84848	1.0959	0.578134	0.004969	B4 B1_B3 B1_B4 B3_B1
62	4	89.594	89.84878	1.0962	0.578047	0.004968	B4 B1_B4 B3_B1 B3_B2
68	5	89.4657	89.85032	1.097738	0.577603	0.004964	B1 B2 B4 B1_B3 B3_B4
70	5	89.4696	89.85422	1.101638	0.576477	0.004955	B2 B4 B1_B2 B1_B3 B2_B4
64	4	89.6057	89.86048	1.1079	0.574675	0.004939	B3 B4 B2_B4 B3_B1
65	4	89.6122	89.86698	1.1144	0.572811	0.004923	B2 B4 B1_B2 B1_B4
58	3	89.7176	89.8695	1.116922	0.572089	0.004917	B4 B3_B4 B3_B1
73	5	89.486	89.87062	1.118038	0.57177	0.004914	B2 B4 B1_B4 B3_B4 B3_B1
67	4	89.6256	89.88038	1.1278	0.568986	0.00489	B4 B1_B4 B3_B4 B3_B1
76	5	89.5069	89.89152	1.138938	0.565826	0.004863	B4 B1_B2 B1_B3 B1_B4 B3_B4
69	4	89.6383	89.89308	1.1405	0.565384	0.004859	B3 B4 B1_B3 B2_B4
74	4	89.66	89.91478	1.1622	0.559283	0.004807	B1 B3 B4 B2_B4
60	2	89.8452	89.92067	1.168095	0.557637	0.004793	B4 B1_B2
75	4	89.6667	89.92148	1.1689	0.557412	0.004791	B2 B4 B1_B4 B2_B1
71	3	89.7866	89.9385	1.185922	0.552688	0.00475	B2 B4 B2_B1
77	4	89.6842	89.93898	1.1864	0.552556	0.004749	B3 B4 B2_B4 B2_B1

Table C5

Model	K	AIC	AICc	Delta AIC_C (Δ_i)	Relative Likelihood	Akaike (w_i)	Model Variables
81	5	89.5551	89.93972	1.187138	0.552352	0.004747	B3 B4 B1_B2 B1_B4 B3_B4
57	1	89.9162	89.9412	1.188623	0.551942	0.004744	B4
79	4	89.6902	89.94498	1.1924	0.550901	0.004735	B2 B4 B3_B4 B3_B1
80	4	89.7019	89.95668	1.2041	0.547688	0.004707	B4 B1_B2 B1_B4 B2_B3
72	2	89.9016	89.97707	1.224495	0.542131	0.00466	B4 B2_B4
78	3	89.8255	89.9774	1.224822	0.542043	0.004659	B1_B4 B3_B1 B4_B3
82	4	89.7391	89.99388	1.2413	0.537595	0.004621	B2 B4 B1_B4 B3_B4
85	5	89.6197	90.00432	1.251738	0.534796	0.004597	B2 B4 B1_B2 B1_B3 B1_B4
86	5	89.621	90.00562	1.253038	0.534449	0.004594	B3 B4 B1_B2 B2_B4 B3_B4
87	5	89.6257	90.01032	1.257738	0.533194	0.004583	B3 B4 B1_B2 B1_B3 B1_B4
83	4	89.7557	90.01048	1.2579	0.533151	0.004582	B3 B4 B2_B4 B3_B4
90	5	89.6375	90.02212	1.269538	0.530058	0.004556	B4 B1_B3 B2_B4 B3_B4 B3_B1
84	4	89.7745	90.02928	1.2767	0.528163	0.00454	B3 B4 B1_B4 B3_B1
88	4	89.7937	90.04848	1.2959	0.523117	0.004496	B2 B4 B2_B4 B3_B4
89	4	89.797	90.05178	1.2992	0.522255	0.004489	B3 B4 B1_B2 B1_B3
92	4	89.8159	90.07068	1.3181	0.517343	0.004447	B2 B4 B1_B3 B3_B1
97	5	89.6903	90.07492	1.322338	0.516247	0.004437	B2 B4 B1_B3 B2_B4 B2_B1

Table C6

Model	K	AIC	AICc	Delta AIC_C (Δ_i)	Relative Likelihood	Akaike (w_i)	Model Variables
98	5	89.6942	90.07882	1.326238	0.515242	0.004428	B2 B4 B1_B2 B1_B4 B3_B4
101	5	89.6995	90.08412	1.331538	0.513878	0.004417	B4 B1_B2 B2_B3 B2_B4 B3_B4
93	4	89.8298	90.08458	1.332	0.51376	0.004416	B3 B4 B1_B4 B2_B1
102	5	89.7	90.08462	1.332038	0.51375	0.004416	B1 B2 B4 B2_B4 B4_B3
94	4	89.8466	90.10138	1.3488	0.509462	0.004379	B3 B4 B1_B3 B1_B4
95	4	89.8469	90.10168	1.3491	0.509386	0.004378	B4 B1_B2 B2_B4 B4_B2
91	3	89.9505	90.1024	1.349822	0.509202	0.004377	B4 B1_B3 B3_B4
105	5	89.7231	90.10772	1.355138	0.50785	0.004365	B4 B2_B4 B3_B4 B3_B1 B3_B2
99	4	89.8623	90.11708	1.3645	0.505478	0.004345	B1_B2 B1_B3 B2_B4 B4_B3
104	4	89.8861	90.14088	1.3883	0.499499	0.004293	B1 B2 B4 B2_B3
106	4	89.8912	90.14598	1.3934	0.498227	0.004282	B1 B3 B4 B1_B4
100	3	90.0021	90.154	1.401422	0.496232	0.004265	B4 B2_B4 B3_B4
103	3	90.0198	90.1717	1.419122	0.49186	0.004228	B2 B4 B1_B2
108	5	89.7878	90.17242	1.419838	0.491684	0.004226	B2 B4 B1_B3 B2_B4 B3_B1
96	2	90.097	90.17247	1.419895	0.49167	0.004226	B4 B1_B4
107	4	89.9215	90.17628	1.4237	0.490735	0.004218	B2 B4 B1_B3 B2_B1
109	5	89.8132	90.19782	1.445238	0.485479	0.004173	B1 B2 B4 B2_B4 B3_B1
120	6	89.6569	90.19884	1.446258	0.485231	0.004171	B1 B2 B4 B2_B3 B2_B4 B3_B4

Table C7

Model	K	AIC	AICc	Delta AIC_C (Δ_i)	Relative Likelihood	Akaike (w_i)	Model Variables
119	5	89.8464	90.23102	1.478438	0.477487	0.004104	B1 B2 B4 B1_B4 B4_B3
111	4	89.9797	90.23448	1.4819	0.476661	0.004097	B2 B4 B1_B2 B1_B3
113	4	89.9837	90.23848	1.4859	0.475709	0.004089	B4 B1_B3 B2_B4 B2_B1
121	5	89.8592	90.24382	1.491238	0.47444	0.004078	B2 B4 B1_B3 B1_B4 B2_B1
116	4	90.0017	90.25648	1.5039	0.471446	0.004052	B3 B4 B1_B4 B3_B4
117	4	90.0032	90.25798	1.5054	0.471093	0.004049	B4 B1_B2 B1_B4 B4_B2
118	4	90.0061	90.26088	1.5083	0.47041	0.004043	B2_B4 B3_B4 B3_B1 B4_B3
110	3	90.1139	90.2658	1.513222	0.469254	0.004033	B2 B4 B3_B4
112	3	90.1185	90.2704	1.517822	0.468176	0.004024	B4 B1_B2 B4_B2
114	3	90.1244	90.2763	1.523722	0.466797	0.004012	B3 B4 B3_B4
115	3	90.1248	90.2767	1.524122	0.466704	0.004011	B4 B1_B2 B2_B3
124	5	89.8975	90.28212	1.529538	0.465441	0.004	B4 B1_B2 B2_B4 B3_B4 B4_B2
132	6	89.7461	90.28804	1.535458	0.464066	0.003989	B1 B2 B4 B1_B3 B1_B4 B3_B4
126	5	89.9115	90.29612	1.543538	0.462195	0.003973	B1 B3 B4 B2_B4 B3_B4
133	6	89.7667	90.30864	1.556058	0.45931	0.003948	B1 B2 B4 B1_B3 B2_B4 B4_B3
127	5	89.9252	90.30982	1.557238	0.459039	0.003945	B1 B2 B4 B2_B4 B4_B1
122	3	90.1611	90.313	1.560422	0.458309	0.003939	B4 B1_B3 B2_B1

Table C8

Model	K	AIC	AICc	Delta AIC_C (Δ_i)	Relative Likelihood	Akaike (w_i)	Model Variables
129	5	89.9302	90.31482	1.562238	0.457893	0.003936	B2 B4 B1_B3 B2_B4 B3_B4
123	4	90.0603	90.31508	1.5625	0.457833	0.003935	B1_B2 B1_B3 B1_B4 B4_B3
131	5	89.9365	90.32112	1.568538	0.456453	0.003923	B3 B4 B2_B4 B3_B4 B3_B1
125	4	90.071	90.32578	1.5732	0.45539	0.003914	B3 B4 B1_B3 B2_B1
128	4	90.0922	90.34698	1.5944	0.450589	0.003873	B2 B4 B1_B3 B3_B4
134	5	89.9658	90.35042	1.597838	0.449815	0.003866	B2 B4 B1_B3 B1_B4 B3_B1
130	4	90.0977	90.35248	1.5999	0.449351	0.003862	B3 B4 B1_B2 B3_B4
135	5	89.9723	90.35692	1.604338	0.448355	0.003854	B1 B2 B4 B1_B4 B3_B1
138	5	89.9793	90.36392	1.611338	0.446789	0.00384	B4 B1_B2 B1_B4 B2_B3 B3_B4
139	5	89.9864	90.37102	1.618438	0.445206	0.003827	B2 B4 B1_B4 B3_B4 B2_B1
140	5	89.9887	90.37332	1.620738	0.444694	0.003822	B2 B4 B1_B2 B2_B4 B3_B4
136	4	90.135	90.38978	1.6372	0.441049	0.003791	B4 B1_B3 B3_B4 B3_B1
137	3	90.2744	90.4263	1.673722	0.433068	0.003722	B4 B2_B3 B3_B1
142	4	90.1863	90.44108	1.6885	0.42988	0.003695	B1 B3 B4 B1_B3
141	3	90.2929	90.4448	1.692222	0.42908	0.003688	B4 B1_B2 B3_B4
143	4	90.1982	90.45298	1.7004	0.427329	0.003673	B1 B2 B4 B3_B1
149	5	90.0714	90.45602	1.703438	0.426681	0.003667	B4 B1_B2 B1_B3 B2_B4 B4_B2

Table C9

Model	K	AIC	AICc	Delta AIC_C (Δ_i)	Relative Likelihood	Akaike (w_i)	Model Variables
144	4	90.2022	90.45698	1.7044	0.426476	0.003666	B4 B1_B2 B2_B4 B3_B1
151	5	90.0734	90.45802	1.705438	0.426254	0.003664	B4 B1_B2 B1_B4 B3_B4 B4_B2
152	5	90.0742	90.45882	1.706238	0.426084	0.003662	B2 B4 B2_B4 B3_B4 B2_B1
153	5	90.0743	90.45892	1.706338	0.426063	0.003662	B3 B4 B1_B3 B2_B4 B2_B1
155	5	90.0791	90.46372	1.711138	0.425041	0.003653	B3 B4 B2_B4 B3_B4 B2_B1
156	5	90.0857	90.47032	1.717738	0.423641	0.003641	B1 B2 B4 B1_B4 B4_B1
147	4	90.2231	90.47788	1.7253	0.422042	0.003627	B4 B3_B4 B3_B1 B3_B2
145	3	90.341	90.4929	1.740322	0.418884	0.0036	B3 B4 B4_B1
168	6	89.9609	90.50284	1.750258	0.416808	0.003582	B3 B4 B1_B2 B1_B3 B2_B4 B3_B4
146	3	90.3544	90.5063	1.753722	0.416087	0.003576	B4 B2_B1 B3_B1
160	4	90.2592	90.51398	1.7614	0.414493	0.003563	B1 B2 B4 B4_B3
148	3	90.3637	90.5156	1.763022	0.414157	0.00356	B1 B4 B3_B1
150	3	90.3655	90.5174	1.764822	0.413784	0.003556	B1_B3 B3_B1 B4_B3
163	4	90.2647	90.51948	1.7669	0.413354	0.003553	B4 B1_B3 B1_B4 B2_B1
154	3	90.3708	90.5227	1.770122	0.412689	0.003547	B1_B2 B2_B4 B4_B3
166	5	90.1446	90.52922	1.776638	0.411347	0.003536	B3 B4 B1_B3 B2_B4 B3_B4
157	3	90.3801	90.532	1.779422	0.410775	0.003531	B2 B4 B4_B1

Table C10

Model	K	AIC	AICc	Delta AIC_C (Δ_i)	Relative Likelihood	Akaike (w_i)	Model Variables
169	5	90.1531	90.53772	1.785138	0.409602	0.003521	B1 B2 B4 B2_B3 B3_B4
158	3	90.3865	90.5384	1.785822	0.409462	0.003519	B1_B3 B2_B4 B4_B3
174	6	89.9993	90.54124	1.788658	0.408882	0.003514	B1 B2 B4 B1_B3 B1_B4 B4_B3
159	3	90.391	90.5429	1.790322	0.408542	0.003511	B3 B4 B4_B3
171	5	90.1612	90.54582	1.793238	0.407947	0.003506	B1 B3 B4 B1_B3 B2_B4
162	3	90.3965	90.5484	1.795822	0.40742	0.003502	B4 B3_B1 B4_B1
164	4	90.3031	90.55788	1.8053	0.405494	0.003485	B1_B3 B2_B4 B3_B1 B4_B3
167	4	90.307	90.56178	1.8092	0.404704	0.003478	B4 B2_B3 B2_B4 B3_B1
170	4	90.3156	90.57038	1.8178	0.402967	0.003463	B4 B1_B3 B1_B4 B3_B4
161	2	90.5	90.57547	1.822895	0.401942	0.003455	B1_B3 B4_B3
176	5	90.1955	90.58012	1.827538	0.40101	0.003447	B4 B1_B4 B3_B4 B3_B1 B3_B2
165	3	90.4357	90.5876	1.835022	0.399512	0.003434	B3_B4 B3_B1 B4_B3
189	6	90.0461	90.58804	1.835458	0.399425	0.003433	B2 B4 B1_B2 B1_B3 B2_B4 B3_B4
179	5	90.2041	90.58872	1.836138	0.399289	0.003432	B3 B4 B1_B2 B2_B3 B2_B4
182	5	90.2061	90.59072	1.838138	0.39889	0.003428	B1 B4 B1_B2 B1_B3 B2_B4
184	5	90.2131	90.59772	1.845138	0.397496	0.003416	B1 B2 B4 B2_B4 B4_B2
175	4	90.3483	90.60308	1.8505	0.396432	0.003407	B3 B4 B1_B3 B3_B1

Table C11

Model	K	AIC	AICc	Delta AIC_C (Δ_i)	Relative Likelihood	Akaike (w_i)	Model Variables
192	6	90.0624	90.60434	1.851758	0.396183	0.003405	B1 B2 B4 B2_B4 B3_B4 B4_B3
172	3	90.4555	90.6074	1.854822	0.395577	0.0034	B4 B1_B2 B3_B1
180	4	90.3636	90.61838	1.8658	0.393411	0.003381	B3 B4 B3_B4 B3_B1
173	3	90.4668	90.6187	1.866122	0.393348	0.003381	B2_B4 B3_B1 B4_B1
185	4	90.3778	90.63258	1.88	0.390628	0.003357	B3 B4 B1_B3 B3_B4
177	3	90.4868	90.6387	1.886122	0.389434	0.003347	B4 B1_B4 B3_B4
178	3	90.4901	90.642	1.889422	0.388792	0.003342	B1_B2 B1_B4 B4_B3
187	4	90.3881	90.64288	1.8903	0.388621	0.00334	B4 B1_B2 B1_B4 B3_B1
188	4	90.3909	90.64568	1.8931	0.388078	0.003336	B2 B4 B2_B4 B4_B1
190	4	90.3927	90.64748	1.8949	0.387728	0.003333	B4 B2_B4 B3_B1 B4_B1
194	5	90.2645	90.64912	1.896538	0.387411	0.00333	B4 B1_B2 B1_B3 B2_B4 B3_B1
191	4	90.3963	90.65108	1.8985	0.387031	0.003327	B2 B4 B3_B4 B2_B1
183	3	90.501	90.6529	1.900322	0.386679	0.003323	B1_B2 B1_B3 B4_B3
195	5	90.2701	90.65472	1.902138	0.386328	0.00332	B4 B1_B2 B1_B3 B2_B4 B3_B2
207	6	90.1134	90.65534	1.902758	0.386208	0.003319	B1 B2 B4 B1_B4 B2_B3 B3_B4
186	3	90.5118	90.6637	1.911122	0.384596	0.003306	B2 B3_B1 B4_B3
198	5	90.2845	90.66912	1.916538	0.383556	0.003297	B2 B4 B1_B3 B1_B4 B3_B4

Table C12

Model	K	AIC	AICc	Delta AIC_C (Δ_i)	Relative Likelihood	Akaike (w_i)	Model Variables
199	5	90.2857	90.67032	1.917738	0.383326	0.003295	B2 B4 B1_B2 B2_B3 B2_B4
201	5	90.2872	90.67182	1.919238	0.383039	0.003292	B3 B4 B1_B3 B1_B4 B2_B1
181	2	90.5984	90.67387	1.921295	0.382645	0.003289	B3_B1 B4_B1
202	5	90.294	90.67862	1.926038	0.381739	0.003281	B4 B1_B2 B1_B3 B1_B4 B4_B2
204	5	90.2984	90.68302	1.930438	0.3809	0.003274	B3 B4 B1_B2 B1_B3 B3_B4
209	5	90.3055	90.69012	1.937538	0.37955	0.003262	B1 B2 B4 B2_B4 B2_B1
196	4	90.4354	90.69018	1.9376	0.379538	0.003262	B4 B1_B3 B3_B1 B3_B2
197	4	90.4394	90.69418	1.9416	0.37878	0.003256	B1 B2 B4 B4_B1
211	5	90.3114	90.69602	1.943438	0.378432	0.003253	B4 B1_B3 B2_B4 B3_B4 B2_B1
193	3	90.5454	90.6973	1.944722	0.378189	0.003251	B2 B4 B4_B3
200	4	90.4448	90.69958	1.947	0.377759	0.003247	B2 B4 B1_B2 B3_B4
203	4	90.4532	90.70798	1.9554	0.376175	0.003233	B2 B2_B4 B3_B1 B4_B3
205	4	90.4575	90.71228	1.9597	0.375367	0.003226	B2 B4 B3_B1 B3_B2
206	4	90.4577	90.71248	1.9599	0.37533	0.003226	B4 B1_B2 B1_B3 B4_B2
208	4	90.4589	90.71368	1.9611	0.375105	0.003224	B3 B4 B3_B4 B2_B1
215	5	90.3305	90.71512	1.962538	0.374835	0.003222	B3 B4 B1_B4 B3_B4 B2_B1

Table C13

Model	K	AIC	AICc	Delta AIC_C (Δ_i)	Relative Likelihood	Akaike (w_i)	Model Variables
218	5	90.3389	90.72352	1.970938	0.373264	0.003208	B3 B4 B1_B2 B1_B4 B2_B3
219	5	90.3392	90.72382	1.971238	0.373208	0.003208	B2 B4 B1_B2 B1_B3 B3_B4
212	4	90.4698	90.72458	1.972	0.373066	0.003206	B1 B3 B4 B3_B4
221	5	90.3403	90.72492	1.972338	0.373003	0.003206	B3 B4 B1_B4 B3_B4 B3_B1
223	5	90.3448	90.72942	1.976838	0.372165	0.003199	B1 B2 B3 B4 B2_B4
224	5	90.347	90.73162	1.979038	0.371755	0.003195	B4 B1_B2 B2_B4 B3_B4 B3_B1
225	5	90.3483	90.73292	1.980338	0.371514	0.003193	B1 B2 B4 B1_B3 B4_B3
213	4	90.4783	90.73308	1.9805	0.371484	0.003193	B1_B4 B3_B4 B3_B1 B4_B3
226	5	90.3529	90.73752	1.984938	0.37066	0.003186	B4 B1_B3 B2_B4 B3_B1 B3_B2
235	6	90.2017	90.74364	1.991058	0.369528	0.003176	B1 B2 B4 B1_B4 B3_B4 B4_B3
216	4	90.4902	90.74498	1.9924	0.36928	0.003174	B2 B4 B1_B4 B4_B1
210	3	90.5952	90.7471	1.994522	0.368889	0.003171	B1_B4 B3_B1 B4_B1
236	6	90.2059	90.74784	1.995258	0.368753	0.003169	B2 B4 B1_B2 B1_B3 B1_B4 B3_B4
217	4	90.4933	90.74808	1.9955	0.368708	0.003169	B2_B4 B3_B1 B3_B2 B4_B3
229	5	90.3676	90.75222	1.999638	0.367946	0.003162	B1 B4 B1_B2 B1_B3 B1_B4